

Recycling of subducted carbonates: Formation of the Taohuala Mountain carbonatite, North China Craton

Shuo Xue^{a,b,f}, Ming-Xing Ling^{a,e,*}, Yu-Long Liu^{b,**}, Weidong Sun^{c,d,e}

^a State Key Laboratory of Isotope Geochemistry, Guangzhou Institute of Geochemistry, Chinese Academy of Sciences, Guangzhou 510640, China

^b CAS Key Laboratory of Mineralogy and Metallogeny, Guangzhou Institute of Geochemistry, Chinese Academy of Sciences, Guangzhou 510640, China

^c Center of Deep Sea Research, Institute of Oceanology, Chinese Academy of Sciences, Qingdao 266071, China

^d Laboratory for Marine Mineral Resources, Qingdao National Laboratory for Marine Science and Technology, Qingdao 266237, China

^e CAS Center for Excellence in Tibetan Plateau Earth Sciences, Chinese Academy of Sciences, Beijing 100101, China

^f University of Chinese Academy of Sciences, Beijing 100094, China

ARTICLE INFO

Keywords:

Taohuala Mountain
North China Craton (NCC)
Carbonatite
Earth's carbon cycle
Subduction

ABSTRACT

Carbonatitic magmatism plays a significant role in Earth's carbon cycle, which is also a lithoprobe of crust-mantle interaction, mantle metasomatism and partial melting. Due to different mineral assemblages and geochemical compositions, and diverse tectonic settings, the origin of carbonatite has long been debated. At subduction zones, sediments (including carbonates) are subducted into the mantle with the downgoing oceanic slab. However, the detailed mechanism of how subducted carbonates contribute to carbonatitic magmatism remains unclear. Here we present geochronological, geochemical and isotopic study on the Taohuala Mountain carbonatite at the southern margin of the Alxa Block, North China Craton. The classification of carbonatite from the Taohuala Mountain relies strongly on the observations of obvious intrusion contact relationships and flow structures in field outcrop. The Taohuala Mountain carbonatite has SiO_2 ranging from 2.37 wt.% to 11.45 wt%, high CaO (45.93–53.86 wt%) and low MgO (0.51–4.39 wt%), and is characterized by enrichment of LILE (Ba, Sr), depletion of HFSE (Nb, Ta, Zr, Hf), and slightly negative Ce and Eu anomalies. Carbonates in the samples have high $^{87}\text{Sr}/^{86}\text{Sr}$ (0.70686–0.70694) and low $^{143}\text{Nd}/^{144}\text{Nd}$ (0.511635–0.511924). Remarkably, the highly fractionated $\delta^{18}\text{O}_{\text{VSMOW}}$ (11.83–25.92‰) indicates components of both sedimentary and mantle origin. Detailed zircon *in situ* U-Pb dating and oxygen isotope analysis exhibit contrast ages and $\delta^{18}\text{O}_{\text{VSMOW}}$ from core to rim, i.e., old ages (mainly > 800 Ma), high Th/U (mainly > 0.5) and low $\delta^{18}\text{O}_{\text{VSMOW}}$ (6.37–11.44‰) in cores (inherited), whereas young ages (~400 Ma), low Th/U (mainly < 0.01) and high $\delta^{18}\text{O}_{\text{VSMOW}}$ (20.04–24.54‰) in rims, suggesting that the Taohuala Mountain carbonatite may have been generated from melting of subducted sedimentary carbonates. Considering all these evidences, and that the collision along Qilian Mountains was older than the carbonatite, we propose that a large volume of sedimentary carbonates subducted and remained in the lithospheric mantle under the Alxa block during the closure of the Paleo-Qilian Ocean. Subsequently, the carbonatite was formed by melting of carbonates with minor contributions from the mantle during the breakup or rollback of the Paleo-Asian oceanic slab.

1. Introduction

The Earth's deep carbon cycle mainly includes carbon input through plate subduction and carbon releasing by volcanic degassing or magmatic processes (e.g. carbonatitic magmatism) (Barker, 1996; Li et al., 2016; Sun and Zhang, 2017; Yang et al., 2012; Zhang et al., 2017). Over a long period of Earth's history, basaltic crust, sediments (including carbonates) and underlying lithospheric mantle, take carbon into the mantle and contribute to mantle heterogeneities through the

subduction process.

Carbonatites are widely distributed in different tectonic settings (e.g. divergent zones, convergent zones, and hot spots). In general, three petrogenetic models have been proposed for carbonatites, including: 1) derivation of parental magmas by direct melting of a carbonate-bearing mantle (Chakhmouradian, 2006; Harmer and Gittins, 1998; Sweeney, 1994); 2) immiscible separation of carbonate and alkaline silicate melts from an initially homogeneous magma (Halama et al., 2005; Ivanov et al., 2010); 3) derivation of CO_2 -rich silicate

* Correspondence to: M.-X. Ling, State Key Laboratory of Isotope Geochemistry, Guangzhou Institute of Geochemistry, Chinese Academy of Sciences, Guangzhou 510640, China.

** Correspondence to: Y.-L. Liu, CAS Key Laboratory of Mineralogy and Metallogeny, Guangzhou Institute of Geochemistry, Chinese Academy of Sciences, Guangzhou 510640, China

E-mail addresses: mxling@gig.ac.cn (M.-X. Ling), ylliu@gig.ac.cn (Y.-L. Liu).

magmas by crystal fractionation (Tappe et al., 2012; Veksler et al., 1998). These models could be used to explain the genesis of most of carbonatite, but have difficulties to interpret carbonatites from Bayan Obo, Hannuoba and Dalihu in North China Craton (NCC) (Chen et al., 2016; Fan et al., 2016; Ling et al., 2013; Liu et al., 2008; Liu et al., 2015; Mitchell, 2005; Yang et al., 2017; Yang et al., 2009). Many researchers have paid attention to the genetic relationship between carbonatite and recycled carbonates (Barker, 1996; Bell and Simonetti, 2010; Chen et al., 2016; Halama et al., 2008; Hoernle et al., 2002; Hou et al., 2015; Hou et al., 2006; Liu et al., 2015; Lu et al., 2013; Song et al., 2016; Woodard and Huhma, 2015; Woodhead, 1996; Xu et al., 2015). However, the detailed process is still unclear regarding how the recycled carbonates contribute to carbonatitic magmas in subduction zones.

Here we present field observation, mineralogy, whole rock major and trace elements, C-O-Sr-Nd isotopic compositions and zircon U-Pb dating and O isotopic composition of the Taohuala Mountain carbonatite from NCC, aiming at better constraints on its petrogenesis, e.g., contribution of subducted carbonates to carbonatitic magmatism. All evidences indicate that the Taohuala Mountain carbonatite was formed by recycling of subducted carbonates at shallow depths.

2. Geological background and samples

The Taohuala Mountain is located in the south margin of Alxa Block, NCC (Fig. 1). The Alxa block is situated in the convergent zone between the Tarim Craton and the NCC, and adjoins the Qilian Orogenic Belt in the south and the Central Asia Orogenic Belt in the north. The tectonic setting of this area is complicated (Chen et al., 2010; Guan et al., 2010; Liu et al., 2010; Qin et al., 2010b; Song et al., 2013; Song et al., 2006; Sun et al., 2010; Wang et al., 2010; Zhang et al., 2010). There are two major ophiolite belts in the Alxa block: the Engger Us Ophiolite Belt (302 ± 14 Ma) in the north and the Qagan Qulu Ophiolite Belt (275 ± 3 Ma) in the south (Li, 2006; Qin et al., 2010a; Wang et al., 2010; Zheng et al., 2014). A large volume of Phanerozoic granitoids outcrop in the Alxa block from the north to the south. Previous researches show that they were mainly formed between 230 and 450 Ma (Dan et al., 2014; Feng et al., 2013; Geng and Zhou, 2012; Lai et al., 2007; Li et al., 2010a; Li, 2006; Ran et al., 2012; Shi et al., 2012; Wu, 2011; Xue et al., 2017; Zhang et al., 2013; Zheng et al., 2013; Zhou et al., 2016).

The Qilian - Qaidam Mountain system is located in the southern part

of the Alxa block, which tectonically represents a broad orogenic belt between the Alxa and Qaidam blocks. There are, from north to south, the Alxa Block, the North Qilian oceanic-type Suture Zone, the Qilian Block, the North Qaidam continental-type ultrahigh pressure metamorphic Belt and the Qaidam Block. The North Qilian oceanic-type Suture Zone consisted with ophiolitic melanges and high-pressure eclogites and blueschists in the north. The North Qaidam continental-type ultrahigh pressure metamorphic Belt in the south, an ultrahigh pressure (UHP) metamorphic terrane, comprise pelitic and granitic gneisses, eclogites and garnet peridotites (Song et al., 2009; Song et al., 2006).

The strata in Taohuala Mountain area can be divided into sedimentary covers and Paleoproterozoic metamorphic basement. The sedimentary covers are exposed in the southwest of our study area, including the Mesozoic (Jurassic - Cretaceous) - Cenozoic (Neogene - Quaternary) strata. The underlying basement (Longshou Mountain group) mainly consists of metasedimentary rocks (garnet mica schist, muscovite quartz schist and kyanite staurolite mica schist) and granitic gneiss. Detrital zircon grains from the metasedimentary rock have two age populations: ~ 2.01 Ga and ~ 2.15 Ga. Magmatic and metamorphic zircons from the granitic gneiss yield ages of 2.04–2.07 Ga and 1.89–1.93 Ga, which support that the Longshou Mountain Group was mainly formed in the Paleoproterozoic (Gong et al., 2011; Tung et al., 2007). Folds and faults are well developed in the study region, e.g., multiple anticline/syncline and inclined folds. Those northwestward faults and folds extend from several to twenty kilometers.

The Taohuala Mountain carbonatite is situated at the southern margin of Alxa Block, NCC, which intruded into the Precambrian Longshou Mountain Group in the form of dikes or veins, covering an area of ~ 40 km 2 . The carbonatite dykes extend from east to west with the length and width of 12 km and 3 km, respectively. The intrusion contact relationship is obvious between carbonatite veins and wall rocks (Longshou Mountain gneiss) (Fig. 2). Several carbonatite dykes extend in the vertical direction with widths of 0.5–5 m. The emplacement directions cut through the wallrock gneissosity at an angle of $\sim 40^\circ$. Typical flow structure that dark-colour minerals and calcites are arranged along the intrusion direction indicates the process of fluid or magma activities (Fig. 2). Such a large outcrop of carbonatite is rare worldwide. Reconnaissance and drilling had been carried out in 1960's, and P, light REE and Nb mineralization had been reported in the carbonatite in this area (Cui, 1976; Jiang, 1989; Zhang, 1990). In some of these literature, the Taohuala Mountain carbonatite was taken as

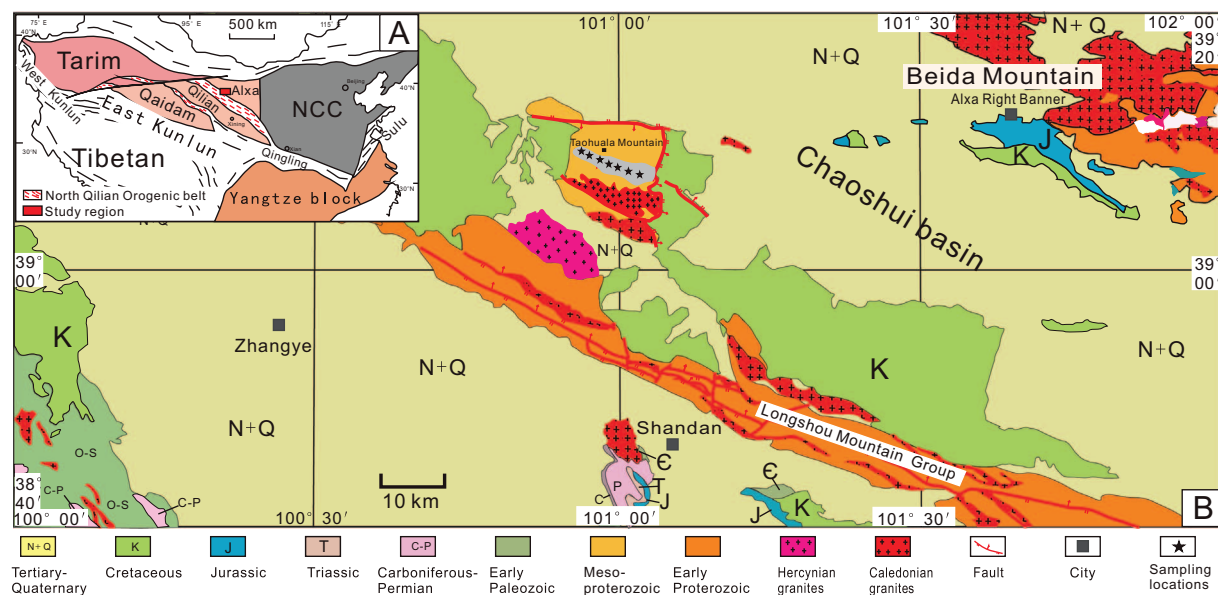


Fig. 1. (A) Tectonic subdivisions of China (Xia et al., 2012). (B) Geological map of the Taohuala Mountain area.

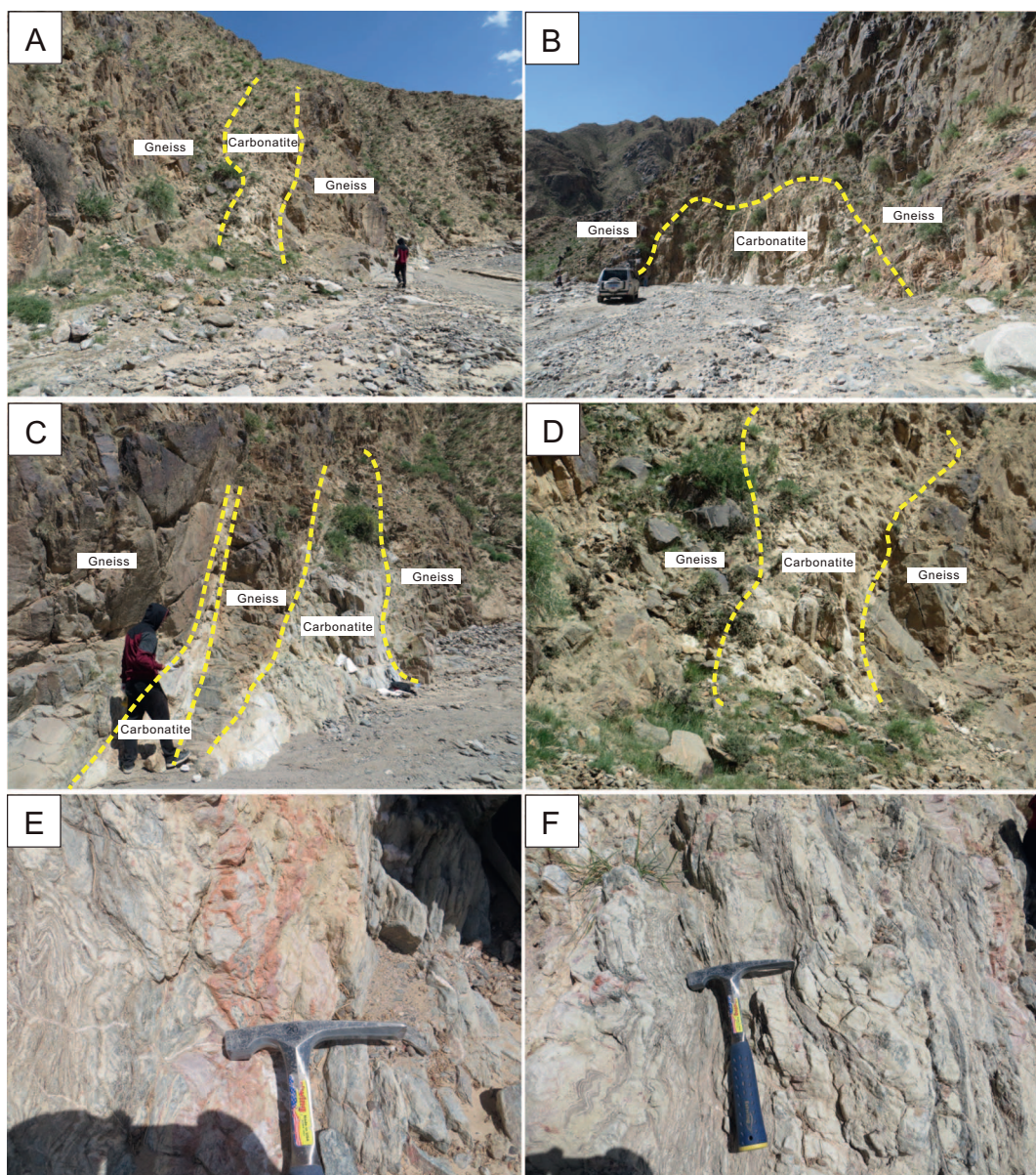


Fig. 2. Field photographs of carbonatite in Taohuala Mountain area. A, B, C and D: Carbonatite veins intrude in the Longshou Mountain genesis with clear contact relationship. E and F: Carbonatite veins show obvious flow structure of magmatic origin.

Longshou Mountain metamorphic marble, which is, however, not consistent with our field observation (Fig. 2) and trace element characteristics (e.g., high Sr, see details below). The carbonatite samples collected in this study are fresh, white and of massive structure, mainly consist of calcite (~90 vol%), biotite (3–5 vol%) and quartz (4–5 vol %), with accessory minerals such as garnet, diopside, amphibole and zircon (Fig. 3). The wall rock (gneiss) consists mainly of quartz (50–60 vol%), biotite (30–40 vol%), feldspar (10 vol%) and minor accessory minerals (e.g., garnet).

3. Analytical methods

3.1. Major and trace element analyses

Fresh carbonatite samples were ground to 200 mesh for major and trace element analysis. Analyses of major and trace elements were performed at the State Key Laboratory of Isotope Geochemistry, Guangzhou Institute of Geochemistry, Chinese Academy of Sciences (SKLIG-GIGCAS). Samples powder was fluxed with $\text{Li}_2\text{B}_4\text{O}_7$ (1:8) to

make homogeneous glass disks for X-ray fluorescence (XRF) analysis, at 1150–1200 °C using a V8C automatic fusion machine (Analymate, China). Major elements were determined by Rigaku 100e XRF with analytical precision better than 1% (Ma et al., 2007). For trace element analyses, about 40 mg powders of each sample were accurately weighed and dissolved by a HF and HNO_3 mixture in screw-top Teflon beakers for 7 days at 120 °C in a clean laboratory. Sample solutions were dried and diluted to 3% HNO_3 with a factor of 1/2000. Rh was used as an internal standard for calibration. The trace elements of these samples were analyzed using a Perkin-Elmer ELAN 6000 ICP-MS with precision better than 5% (Liu et al., 1996).

3.2. Zircon SIMS oxygen isotope analysis

Zircons were separated from samples by traditional heavy liquid and magnetic separation techniques, handpicked under a binocular microscope, mounted with epoxy resin and then polished down to near half sections to expose internal structures for SIMS analyses (Fig. 4). Cathodoluminescence (CL) and microscopic images were used to

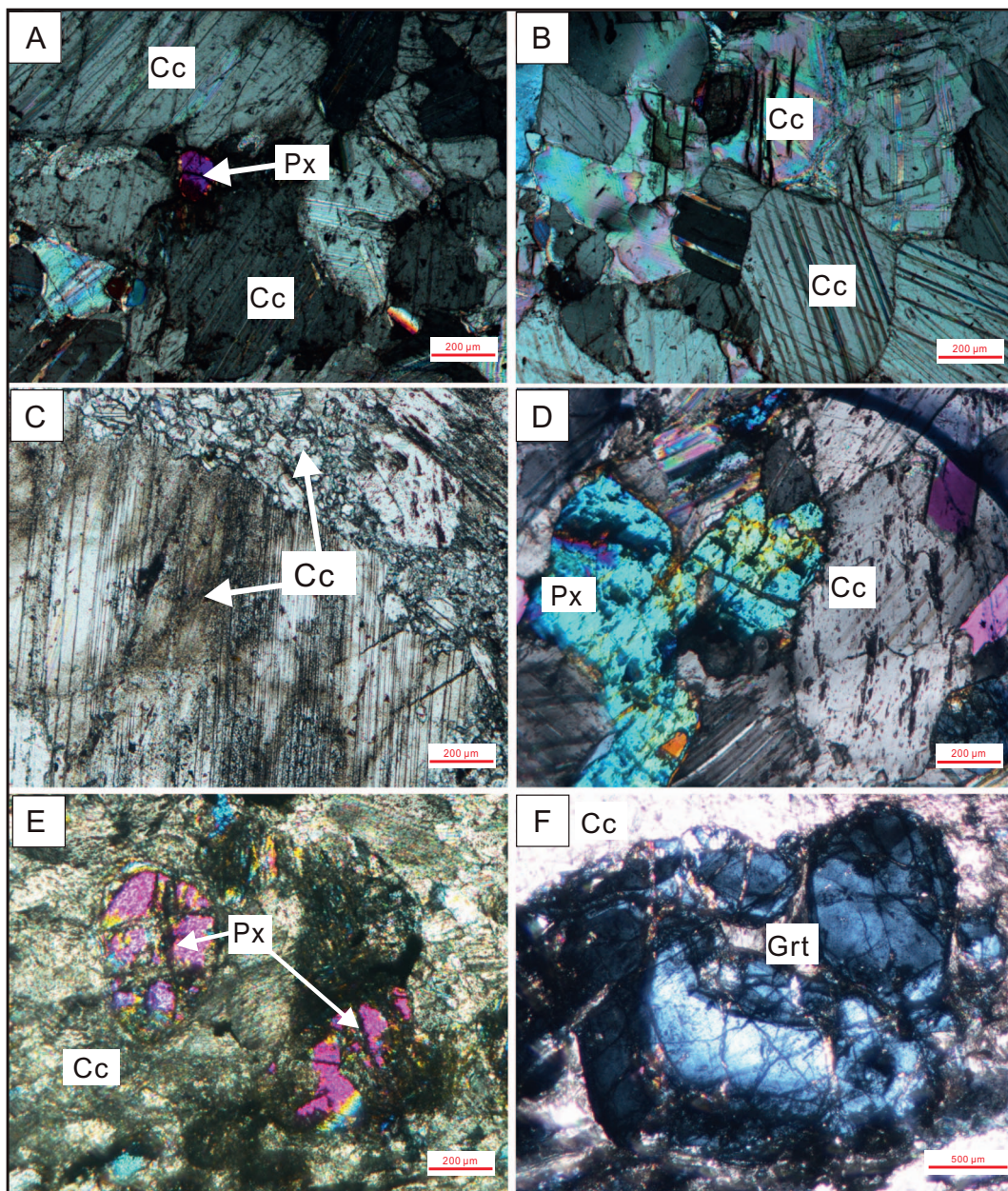


Fig. 3. Photomicrographs (cross-polarized light) of carbonatite in Taohuala Mountain area. A, B, C, D, E and F: The micrographs of Taohuala Mountain carbonatites. Cc = calcite, Px = pyroxene, Grt = garnet.

inspect the zircon morphology and the clearest, least fractured rims of the zircon crystals were selected as suitable targets for laser ablation. Zircon oxygen isotopes were measured using the Cameca IMS-1280 SIMS at the SKLIG-GIGCAS. Measurements were made using a primary beam of $^{133}\text{Cs}^+$ ions accelerated at 10 kV, with an intensity of ~ 2 nA, rastered over a 10 μm area. An electron flood gun was used for charge compensation during analysis. Oxygen isotopes, ^{18}O and ^{16}O , were measured simultaneously in multi-collector mode using two off-axis Faraday cups. Measured $^{18}\text{O}/^{16}\text{O}$ ratios were normalized by using Vienna Standard Mean Ocean Water (VSMOW), and then corrected for the instrumental mass fractionation factor, which is corrected using zircon 91500 as a reference with a $\delta^{18}\text{O}$ value of 9.9‰ (Wiedenbeck et al., 2004). The detailed analytical procedures were similar to those described by Li et al. (2010b).

The measured oxygen isotopic data were corrected for instrumental mass fractionation using the “Qinghu” and “Penglai” zircon standard (Li et al., 2010b). The internal precision of a single analysis generally

was better than 0.2‰ (1σ standard error) for the $^{18}\text{O}/^{16}\text{O}$ ratio. The external precision, measured by the reproducibility of repeated analyses of Penglai standard is 0.50‰ (2SD, $n = 68$).

3.3. Zircon SIMS U-Pb dating

Zircon U-Pb dating of the samples was performed at the SKLIG-GIGCAS, using the same Cameca IMS 1280 SIMS following the procedures reported by (Li et al., 2009). U-Th-Pb ratios and their absolute abundances were determined relative to the standard zircon Plešovice and Qinghu, respectively. The O^{2-} primary ion beam was accelerated at 13 kV, with an intensity of ca. 8 nA. The ellipsoidal spot is about $20 \times 30 \mu\text{m}$ in size. Positive secondary ions were extracted with a 10 kV potential. A mass resolution of ca. 5400 was used to separate Pb^+ peaks from isobaric interferences. A single electron multiplier was used in ion-counting mode to measure secondary ion beam intensities by peak jumping. Each measurement consists of 7 cycles. A long-term

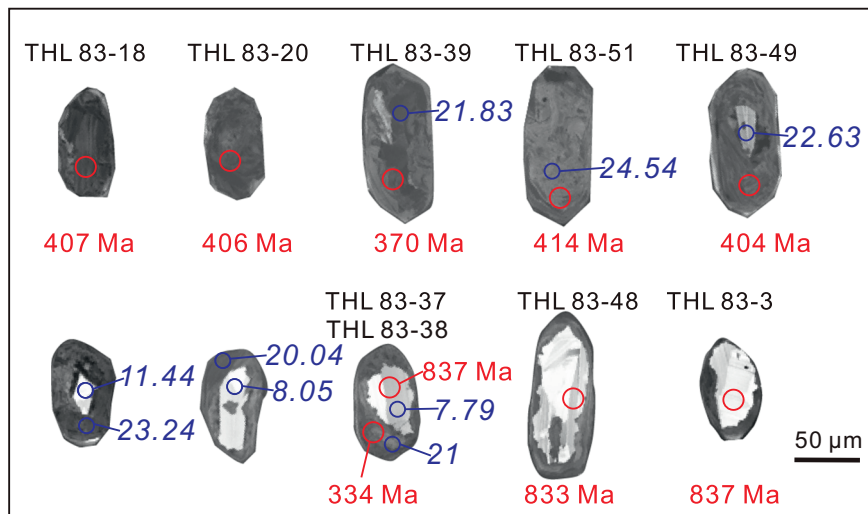


Fig. 4. Representative cathodoluminescence (CL) images of zircons from carbonatite of the Taohuala Mountain analyzed in situ for U-Pb dating and O isotopic analysis. Solid red circles indicate SIMS analysis spots for U-Pb dating. The solid blue circles indicate O analysis points. The marked ages for zircons (red numbers) represent ages of $^{206}\text{Pb}/^{238}\text{U}$. The blue numbers represent the value of O isotope. (For interpretation of the references to colour in this figure legend, the reader is referred to the web version of this article.)

uncertainty of 1.5% (1 RSD) for $^{206}\text{Pb}/^{238}\text{U}$ measurements of the standard zircons was propagated to the unknowns (Li et al., 2010b), despite the measured $^{206}\text{Pb}/^{238}\text{U}$ error during the course of this study generally is around 1% (1 RSD) or less. Measured compositions were corrected for common Pb using non-radiogenic ^{204}Pb . Corrections were sufficiently small to be insensitive to the choice of common Pb composition, and an average of present-day crustal composition (Stacey and Kramers, 1975) was used for the common Pb, assuming that the common Pb was largely surface contamination introduced during sample preparation. Uncertainties on individual analyses in the data tables are reported at a 1σ level. Mean ages for pooled U/Pb and Pb/Pb analyses are quoted with 2σ and/or 95% confidence intervals. Data reduction was carried out using the Isoplot/Ex v.3.0 program (Ludwig, 2012).

3.4. Whole rock C-O isotope analysis

The $\delta^{13}\text{C}$ and $\delta^{18}\text{O}$ of carbonates were analyzed by a continuous flow Isoprime 100 stable isotope ratio mass spectrometer (IRMS) coupled with a MultiFlow device in the SKLIG-GIGCAS. About 0.1–0.2 mg sample powder was flushed by pure He (99.999%), dissolved with excess (5–7 drops) 102% H_3PO_4 at 90 °C, analyzed by IRMS. Samples were analyzed in duplicate. The $\delta^{13}\text{C}$ and $\delta^{18}\text{O}$ results were reported in standard delta notation (‰ units) relative to the Vienna Pee Dee Belemnite (V-PDB), and corrected to 25 °C. Two Chinese isotopic standards GBW04405 and GBW04406 together with an international isotopic standard IAEA-CO-8 were analyzed between each 5 samples. A three-point correction method ($r > 0.999$) both for $\delta^{13}\text{C}$ and $\delta^{18}\text{O}$, based on the standards IAEA-CO-8, GBW04405 and GBW04406, was applied in this study, which is better than the two-point correction method and can greatly reduce the uncertainties in the results. The results of duplicate analysis indicate that the external precision is better than 0.10‰ (1σ) for $\delta^{13}\text{C}$, and 0.15‰ (1σ) for $\delta^{18}\text{O}$.

3.5. Sr-Nd isotope analysis

Sr and Nd isotope analysis of carbonates in the Taohuala Mountain carbonatite were made using a multi-collector inductively coupled plasma mass spectrometry (MC-ICP-MS) at the SKLIG-GIGCAS, after the routine procedures (Liang et al., 2003; Wei et al., 2002). The $^{87}\text{Sr}/^{86}\text{Sr}$ and $^{143}\text{Nd}/^{144}\text{Nd}$ were calculated from the Rb, Sr, Sm and Nd contents measured by ICP-MS. Measured $^{87}\text{Sr}/^{86}\text{Sr}$ and $^{143}\text{Nd}/^{144}\text{Nd}$ values were normalized to $^{87}\text{Sr}/^{86}\text{Sr} = 0.1194$ and $^{146}\text{Nd}/^{144}\text{Nd} = 0.7129$ for mass fractionation. Long-term mean values

of the Sr and Nd standards NBS 987 and JNd-1 of the laboratory are $^{87}\text{Sr}/^{86}\text{Sr} = 0.710249 \pm 0.000005$ and $^{143}\text{Nd}/^{144}\text{Nd} = 0.512112 \pm 0.000004$, respectively.

3.6. EPMA analysis

In situ chemical analysis and back-scattered electron (BSE) imaging of minerals were carried out using a JEOL JXA-8100 Superprobe at the SKLIG-GIGCAS. The operating conditions are: 15 kV accelerating voltage, 20 nA beam current, 1–2 μm beam diameter, and 10 s peak counting time for most elements. The data reduction was carried out using ZAF correction.

4. Results

4.1. Whole rock major and trace element compositions

The carbonatite samples have high CaO (45.93–53.86 wt%), low MgO (0.51–4.39 wt%) and low alkali contents ($\text{Na}_2\text{O} + \text{K}_2\text{O} < 0.57$ wt%). In the $\text{CaO}-\text{MgO}-\text{Fe}_2\text{O}_3^{\text{T}} + \text{MnO}$ diagram, the Taohuala Mountain carbonatite plots in the field of calciocarbonatite (Fig. 5). The samples have high similarity in trace element characteristics with sedimentary carbonate, e.g., notably positive Sr and U anomalies and negative HFSE (Nb, Ta, Zr, Hf) anomalies. The trace element concentrations of most samples, however, are 5–10 times higher than average value of carbonate (Fig. 6). Total REE concentrations range from 7.39–65.4 ppm. LREE are weakly enriched in the chondrite-normalized REE diagram, with LREE/HREE ranging from 1.7–4.7 and $(\text{La}/\text{Yb})_{\text{N}}$ ranging from 5.99–24.0. The carbonatite exhibits a slight negative anomaly ($\delta\text{Eu} = 0.19$ –0.26). The results of major and trace element are given in the Table S1.

4.2. C-O-Sr-Nd isotopic compositions

The C-O isotopic compositions of the Taohuala Mountain carbonatite vary widely, with $\delta^{13}\text{C}_{\text{VPDB}}$ ranging from –2.33‰ to 6.20‰ and $\delta^{18}\text{O}_{\text{VSMOW}}$ from 11.83‰ to 25.92‰ (Table 1). Carbonates in the Taohuala Mountain carbonatite have high and homogeneous $^{87}\text{Sr}/^{86}\text{Sr}$ (0.706286–0.706940), and low and relatively varied $^{143}\text{Nd}/^{144}\text{Nd}$ (0.511635–0.511924) (Table 2), similar to those of sedimentary limestone (Veizer et al., 1999).

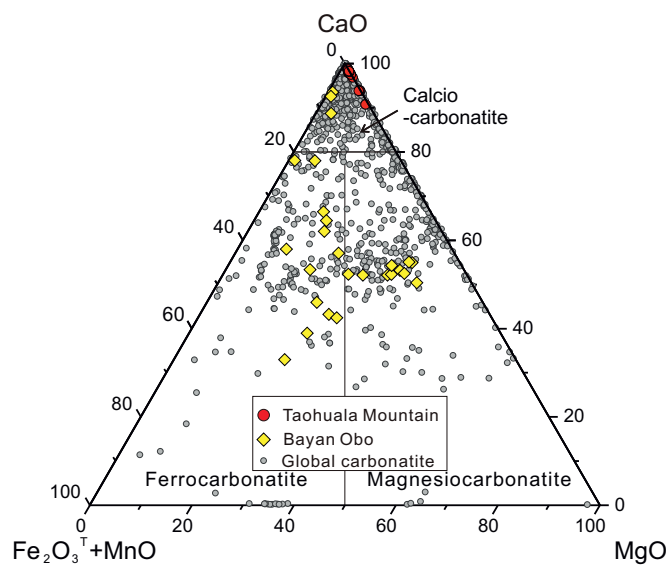


Fig. 5. CaO-MgO- $\text{Fe}_2\text{O}_3^{\text{T}} + \text{MnO}$ diagram (Woolley, 1989) of Taohuala Mountain carbonatite intrusion (red circles). Bayan Obo data are from Ling et al. (2013). Global carbonatite data are from GEOROC. (For interpretation of the references to colour in this figure legend, the reader is referred to the web version of this article.)

4.3. Zircon U-Pb dates and oxygen isotopic composition

Zircon from carbonatite samples (THL 83 and THL 84) were selected to perform U-Pb dating and O isotope analysis (Table S2 and 3, Fig. 4). The zircon grains are generally anhedral to subhedral, and a few crystals are short prismatic or irregular in shape. Lengths of these grains range from 50 to 150 μm , with length/width ratios of approximately 1:1 to 3:1. In CL images, zircon grains show unclear oscillatory zoning and cloud internal structure. The Th/U ratios (mainly < 0.01) are low. Inherited old cores show clear magmatic oscillatory zoning and relatively strong brightness. Relatively low U contents (70–835 ppm) and a high Th/U ratios (mainly > 0.5) show that the core have a magmatic origin. Resorption structures are preserved around the cores.

The 95 zircon spots dating analyses were listed in Table S2. Except 25 zircon core age data, others are all concordant in U-Pb ages within 1σ uncertainty, and have a wide $^{206}\text{Pb}/^{238}\text{U}$ age spectra range from 430.7 to 334.4 Ma (Fig. 7). The 70 analyses yield a weighted mean $^{206}\text{Pb}/^{238}\text{U}$ age of 405 ± 21 Ma (MSWD = 0.61). The age of inherited zircon cores have broad Proterozoic age range from 830 Ma to

Table 1
The C-O isotopic composition of Taohuala Mountain carbonatite.

Sample	$\delta^{13}\text{C}$	$\delta^{18}\text{O}$	Sample	$\delta^{13}\text{C}$	$\delta^{18}\text{O}$
THL41	4.69	18.70	THL69	5.07	24.55
THL42	3.31	15.47	THL71	5.52	23.54
THL43	2.11	14.00	THL72	4.65	24.36
THL44	-2.33	16.08	THL73	4.62	23.84
THL45	-1.21	14.10	THL74	5.44	25.89
THL46	4.02	20.57	THL75	5.68	25.00
THL47	4.02	20.32	THL76	5.06	25.09
THL48	3.54	11.83	THL77	5.76	23.08
THL49	3.89	14.51	THL78	5.50	25.31
THL50	-2.25	15.67	THL79	6.05	25.92
THL51	5.07	24.43	THL80	5.37	24.97
THL52	6.03	22.25	THL81	5.67	25.70
THL53	5.27	23.90	THL82	5.76	24.99
THL54	5.35	24.34	THL83	6.20	25.10
THL55	5.26	23.66	THL84	5.86	25.02
THL60	4.48	15.99	THL85	5.15	23.09
THL61	5.00	21.41	THL86	5.32	25.52
THL62	5.19	22.06	THL87	5.82	25.60
THL63	5.42	18.57	THL88	5.17	25.32
THL64	5.55	19.51	THL91	5.49	25.20
THL66	4.91	23.95	THL92	4.62	21.60
THL67	4.91	23.84	THL93	5.94	24.98
THL68	4.69	24.19	THL94	5.54	25.29

2000 Ma. There are three distinct age spectrum peak, e.g., 830 Ma, 1570 Ma, 2000 Ma. Total 20 zircon oxygen isotopes were obtained (including 10 cores analysis, Table 3). All of the cores show relative low $\delta^{18}\text{O}_{\text{VSMOW}}$ (6.37–11.44‰) values, and the rim or non-core zircon display very high $\delta^{18}\text{O}_{\text{VSMOW}}$ (20.04–24.54‰).

5. Discussions

5.1. Petrogenesis of the Taohuala Mountain carbonatite

Except a few occurrences of carbonatites that are enriched in alkalis (i.e., natrocarbonatites), majority of carbonatites can be divided into calciocarbonatite, magnesiocarbonatite and ferrocyanatite based on the chemical compositions (e.g., CaO, MgO and $\text{Fe}_2\text{O}_3^{\text{T}} + \text{MnO}$). The Taohuala Mountain carbonatite plots in the field of calciocarbonatite (calcite > 75 mol%) (Fig. 5), similar to calciocarbonatite from Bayan Obo (Ling et al., 2013). The petrogenesis of the Taohuala Mountain carbonatite has long been debated. It was taken as either metamorphic marble that belongs to the Precambrian Longshou

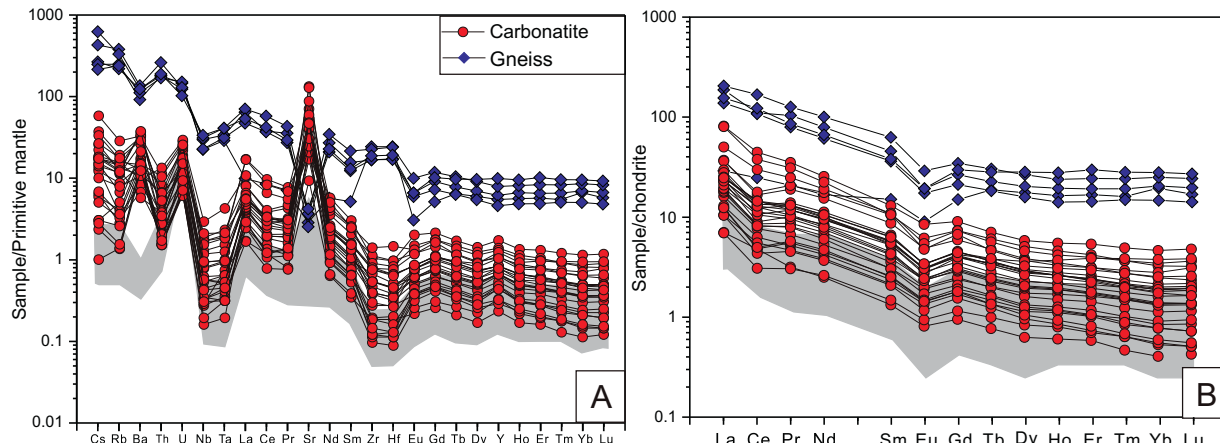


Fig. 6. Primitive-mantle-normalized trace element spider diagram (A) and chondrite-normalized rare earth element pattern (B) of Taohuala Mountain carbonatite (data of this study). The Taohuala Mountain carbonatite samples mark by red cycles and blue diamonds represent the Longshou Mountain gneiss. Grey shadow represents the sedimentary carbonate trace element characteristics (Jin et al., 2009). Normalization values are from Sun and McDonough (1989). (For interpretation of the references to colour in this figure legend, the reader is referred to the web version of this article.)

Table 2
Sr and Nd isotope composition of carbonates in the Taohuala Mountain carbonatite.

Sample	Rb	Sr	Rb/Sr	$^{87}\text{Sr}/^{86}\text{Sr}$	$^{87}\text{Sr}/^{86}\text{Sr}$	2σ	t(Ma)	I_{Sr}	Srn	Nd	Sm/Nd	$^{147}\text{Sm}/^{144}\text{Nd}$	$^{143}\text{Nd}/^{144}\text{Nd}$	2σ	$(^{143}\text{Nd}/^{144}\text{Nd})_i$	$\varepsilon\text{Nd(t)}$	$T_{\text{DM}}(\text{Ma})$
THL48	12.08	1258.3	0.0096033	0.0277738	0.70682	0.00008	400	0.7066598	1.421	7.346	0.1934386	0.1246518	0.511716	0.00006	0.511385397	-14.272404	2305.9
THL49	12.42	1871.1	0.0066378	0.0192072	0.706531	0.000013	400	0.7064202	1.377	8.509	0.1618287	0.1042824	0.511635	0.00004	0.511358421	-14.799157	1988.8
THL53	13.43	3531.7	0.0038027	0.0110035	0.706316	0.00008	400	0.7062525	0.881	4.438	0.1985128	0.1279217	0.511872	0.00006	0.511532725	-11.395563	2074.5
THL55	3.554	3644.8	0.0009751	0.0028215	0.706286	0.00009	400	0.7062697	0.769	3.847	0.199896	0.128813	0.51186	0.00006	0.511518361	-11.676046	2112.6
THL92	9.528	1268.7	0.00751	0.0217311	0.70694	0.00001	400	0.7068147	0.842	4.179	0.2014836	0.129836	0.511924	0.00006	0.511579647	-10.479312	2029.4
THL93	1.224	1237.6	0.000989	0.0028618	0.706385	0.00009	400	0.7063685	0.354	1.955	0.1810742	0.1166842	0.511915	0.00008	0.511605529	-9.9739297	1803.4
																	1958.7

The parameters and corrected equation are as follows: $(^{87}\text{Sr}/^{86}\text{Sr})_i = (^{87}\text{Sr}/^{86}\text{Sr})_s + ^{87}\text{Rb}/^{86}\text{Sr}(e^{\lambda t} - 1)$, $\lambda = 1.42 \times 10^{-11} \text{ a}^{-1}$; $\lambda = 1.42 \times 10^{-11} \text{ a}^{-1}$; $T_{\text{DM}} = 1/\lambda \times \ln\{[(^{143}\text{Nd}/^{144}\text{Nd})_s - (^{143}\text{Nd}/^{144}\text{Nd})_i] / [(^{143}\text{Nd}/^{144}\text{Nd})_{\text{CHUR(t)}} - 1]\} \times 10^4$, $T_{\text{DM}} = 1/\lambda \times \ln\{[(^{143}\text{Nd}/^{144}\text{Nd})_s - (^{143}\text{Nd}/^{144}\text{Nd})_i] / [(^{143}\text{Nd}/^{144}\text{Nd})_{\text{CHUR(t)}} - 1]\}$.

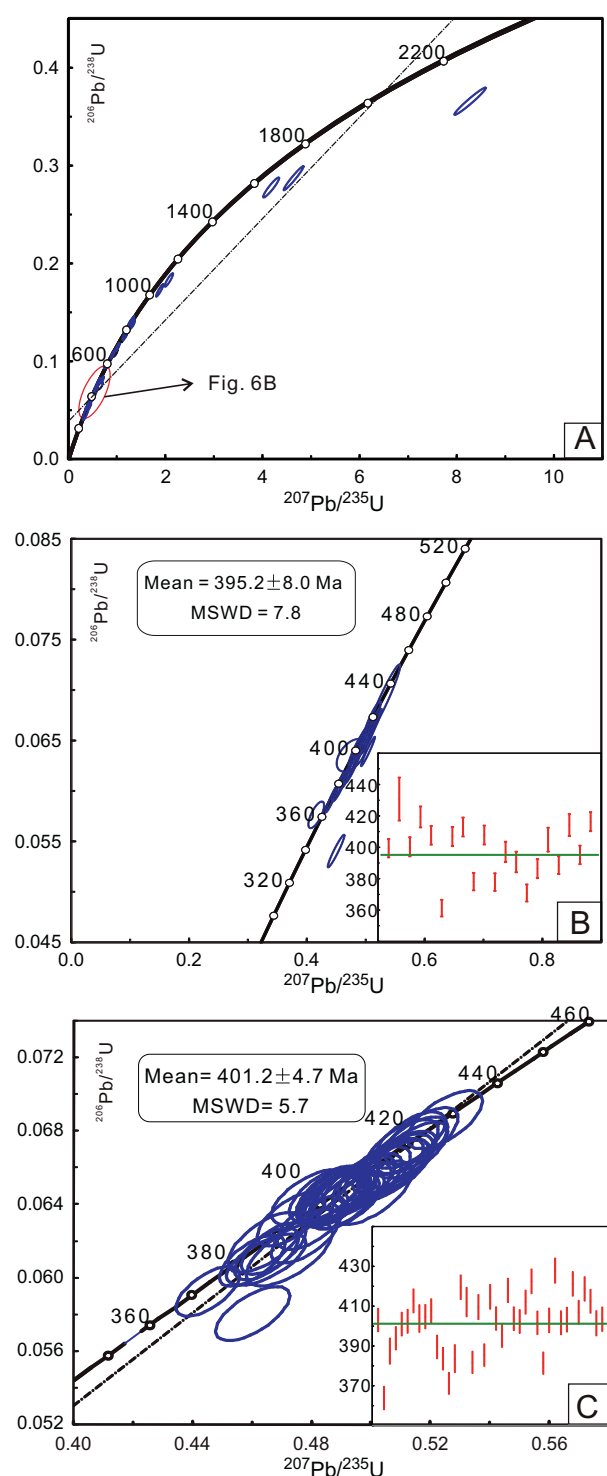


Fig. 7. Zircon SIMS U-Pb Concordia diagrams of zircons in carbonatite from the Taohuala Mountain. A: Concordia diagram of zircons age (rims and cores) from sample THL 83, B: Concordia diagram of metamorphic rims of THL 83, C: Concordia diagram of zircons age from sample THL 84.

Mountain Group (Cui, 1976; Jiang, 1989; Zhang, 1990), or carbonatite dykes (Bai and Yuan, 1985; Yang and Woolley, 2006).

Metamorphic marble was seemingly supported by the following observations: Firstly, the Taohuala Mountain carbonatite is consonant with sedimentary carbonate in trace element patterns (Bellanca et al., 1997; Jin et al., 2009; Tanaka et al., 2003; Tsikos et al., 2001). Secondly, the C-O-Sr-Nd isotope compositions indicate that the Taohuala Mountain carbonatite has a close relationship with sedimentary

Table 3
Zircon O isotopic composition of the Taohuala Mountain carbonatite.

Sample	$\delta^{18}\text{O}_{\text{VSMOW}}$	2SE	Position
THL83-01	24.54	0.18	Rim
THL83-02	10.85	0.15	Core
THL83-03	22.98	0.17	Rim
THL83-04	22.63	0.18	Rim
THL83-05	7.79	0.12	Core
THL83-06	22.18	0.21	Rim
THL83-07	21.83	0.24	Rim
THL83-08	23.26	0.13	Rim
THL83-09	8.05	0.19	Core
THL83-10	20.04	0.23	Rim
THL83-11	8.31	0.15	Core
THL83-12	7.50	0.14	Core
THL83-13	24.53	0.24	Rim
THL83-14	23.24	0.21	Rim
THL83-15	11.44	0.26	Core
THL83-16	7.54	0.12	Core
THL83-17	7.16	0.15	Core
THL83-18	23.49	0.16	Rim
THL83-19	6.37	0.19	Core
THL83-20	6.48	0.20	Core

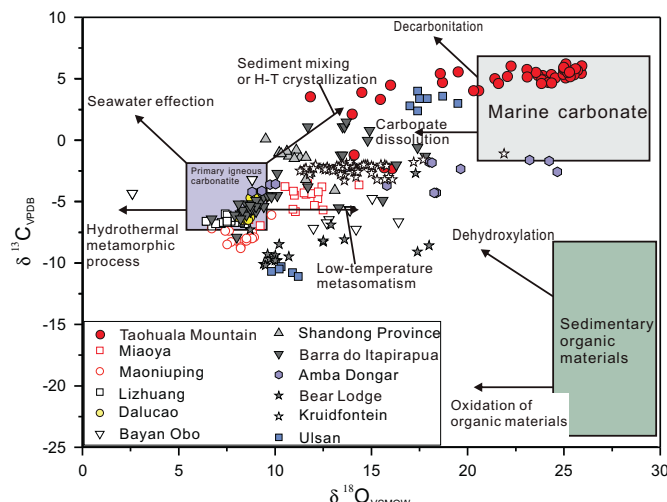


Fig. 8. C–O isotopic composition of the Taohuala Mountain carbonatite (date from this study) and global carbonatites (Table S5). Most samples show the contribution of mantle to the carbonatite source. Mantle and marine sediment boxes for carbonatites from Taylor et al. (1967) and Keller and Hoefs (1995). C–O isotopic data for global carbonatites are from literature (Table S5). Arrows indicate schematically the main processes responsible for change in the C–O isotopic composition (Demény et al., 1998; Taylor et al., 1967).

carbonates. The $\delta^{13}\text{C}_{\text{VPDB}}$ ($-2.33\text{\textperthousand}$ to $6.20\text{\textperthousand}$) and $\delta^{18}\text{O}_{\text{VSMOW}}$ ($11.83\text{\textperthousand}$ to $25.92\text{\textperthousand}$) fall into an intermediate area between primary igneous carbonatite and marine carbonate (Fig. 8).

We argue that the Taohuala Mountain carbonate is carbonatite. Firstly, the field occurrence is one of the major criteria to distinguish carbonatite from marble. Carbonatite usually has ‘intrusive’ occurrence, while marble occurs as ‘sedimentary’. The Taohuala Mountain carbonatite mostly occurs as layers and lenses within metamorphosed sedimentary rocks, seemingly like a marble. However, based on detailed field observation, obvious intrusion contact relationship and flow structure have been found, which strongly indicate a magmatic origin rather than metamorphic sedimentary marble (Fig. 2). Several carbonatite dykes extend in the vertical direction with widths of 0.5–5 m. The emplacement directions have obvious angle ($\sim 40^\circ$) with the gneissosity direction. Typical flow structure that dark-colour minerals and calcites are arranged along the intrusion direction indicates the process of fluid or magma activities (Fig. 2). The Taohuala Mountain carbonatite has low alkaline contents ($\text{Na}_2\text{O} + \text{K}_2\text{O} = 0.13\text{--}0.57\text{ wt\%}$).

The quench margins and wallrock metasomatism are not clearly shown in the field observation. Secondly, carbonate minerals in carbonatite are typically rich in Sr (Dawson et al., 1996). The Sr concentration is an important chemical characteristic to identify carbonatite. For example, SrO contents in carbonate minerals higher than 0.15 wt% are used as indicators to distinguish carbonatite from sedimentary carbonate rocks (Yang and Le Bas, 2004). The average Sr concentration of the Taohuala Mountain carbonatites is 1551 ppm, with several samples (THL 53, THL 54 and THL 55) even exceed 3000 ppm, corresponding to 0.18 wt% and 0.36 wt%, respectively.

Thirdly, the Longshou Mountain gneiss is a set of Proterozoic metamorphic sediments, the zircon ages range between 1100 and 2400 Ma (Xue et al., unpublished materials), which are consistent with previous study (Gong et al., 2011; Tung et al., 2007). The Taohuala Mountain carbonatite zircon ages are obvious younger than that of the wall rock (Longshou Mountain gneiss), supporting the intrusion relationship and flow structure. Niobium, P and REE mineralizations have also been reported in drilling carbonatite samples of Taohuala Mountain (Jiang, 1989). These kinds of deposits are commonly related to carbonatite worldwide, but are rarely associated with marble.

Several genesis models of carbonatite have been proposed (Chakhmouradian, 2006; Halama et al., 2005; Harmer and Gittins, 1998; Ivanov et al., 2010; Sweeney, 1994; Tappe et al., 2012; Veksler et al., 1998). Both liquid immiscibility and crystal fractionation have been invoked to explain derivation of small-volume carbonate melts from a hybrid alkali-rich carbonate–silicate magma (Halama et al., 2005; Van Groos and Wyllie, 1963; Verhulst et al., 2000). These options are preferred because of close spatial relationship between carbonatites and alkali silicate rocks. The Taohuala Mountain carbonatite has no association with alkali silicate rocks. Only Carboniferous adakitic granite was reported in this region, with ages of ~ 330 Ma (Xue et al., 2017), much younger than carbonatitic magmatism (~ 400 Ma). More importantly, immiscibility experiments in compositionally diverse silicate–carbonate systems have demonstrated that Pb, Nb, Th, U and most of the REE partition preferentially into the silicate liquid, whereas Sr, Ba and F into the conjugate carbonate fraction (Jones et al., 1995; Martin et al., 2013; Veksler et al., 2012; Veksler et al., 1998). This pattern of element partitioning is inconsistent with the trace element characteristics of the Taohuala Mountain carbonatite (Table S1 and Fig. 6). Meanwhile, the crystallization differentiation and liquid immiscibility processes may not cause significant C–O–Sr–Nd isotopic fractionations.

C and O isotopic composition of Taohuala Mountain carbonatite

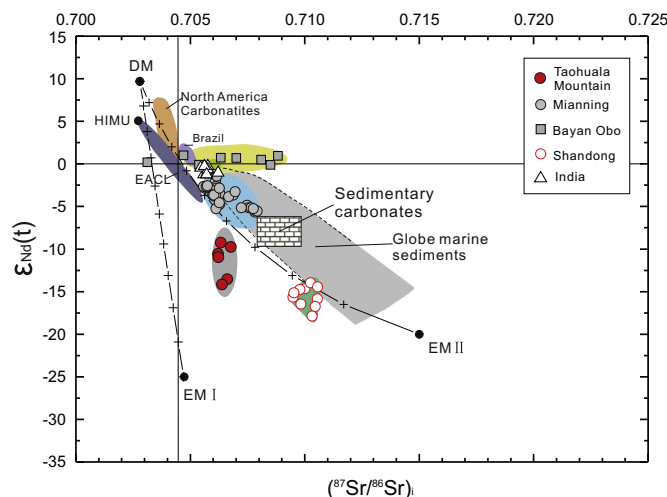


Fig. 9. Diagrams showing $\epsilon_{\text{Nd}}(t)$ versus $(^{87}\text{Sr}/^{86}\text{Sr})_i$. Sr–Nd isotopic compositions of the fresh Taohuala carbonatites and other global carbonatites. Sr–Nd isotopic data for global carbonatites are from literature (Table S6).

indicates a sedimentary carbonate origin with mantle contributions. Meanwhile, high $^{87}\text{Sr}/^{86}\text{Sr}$ (0.70686–0.70694) and varied low $^{143}\text{Nd}/^{144}\text{Nd}$ (0.511635–0.511924) of carbonates in the carbonatite demonstrate close relationship with the marine sediments (Fig. 9). The samples also fall into the mixing line between the mantle and marine carbonates. Therefore, the Taohuala Mountain carbonatite may have generated from partial melting of sedimentary carbonate with minor mantle contribution, consistent with low MgO content (0.51–4.39 wt %).

5.2. Geochronology of the Taohuala Mountain carbonatite

Dating of carbonatite is challenging, in many cases, due to lack of suitable minerals, e.g., zircon and baddeleyite (Rukhlov and Bell, 2010; Woolley and Kjarsgaard, 2008). Recently, apatite was reported to determine ages for carbonatite (Chen and Simonetti, 2013; Chew et al., 2011). Zircon may crystallize from carbonatitic magma, or be captured from the wall rock during carbonatitic magma intrusion process. Thus it is crucial to distinguish captured and carbonatitic zircons.

Most of the zircon grains extracted from the samples (THL 83 and THL 84) show irregular shape, with internal structures of cloud zonation. Several zircon grains have rim-core structures, as indicated by the CL images (Fig. 4). The inherited cores have irregular shape, oscillatory zoning, high Th/U with relatively stronger brightness. The zircon cores may be inherited from protoliths.

Oxygen isotopic and trace element analysis of zircons can provide reliable and robust information of formation environment and constraints on the protoliths of host rocks (Valley, 2003). A large number of studies have shown that zircons preserve their $\delta^{18}\text{O}$ value from the time of crystallization (Moser et al., 2008; Page et al., 2007; Peck et al., 2003; Valley et al., 1994; Watson and Cherniak, 1997). Zircons in the Taohuala Mountain carbonatite have extraordinary high $\delta^{18}\text{O}$ values (20.04–24.54‰). The equilibrium fractionation factor for calcite-zircon calculated from published values for zircon-quartz and quartz-calcite yields $1000 \times \ln \alpha$ (calcite-zircon) = $2.26 \times 10^6 / T^2$ (Valley, 2003). This fractionation factor yields $\Delta^{18}\text{O}_{\text{calcite-zircon}} = 2.0\text{--}3.8\%$ from 800 to 500 °C. These indicate that the high $\delta^{18}\text{O}$ values zircons were crystallized in this carbonatitic environment.

The carbonatite zircon grains have low REE concentration and relative weak REE fractionation (Table S3, Fig. 10). The shallower HREE slope of the majority of zircon grains might be attributed to the appearance of garnet during/before the zircon crystallization. The mineral assemblage (garnet and diopside) indicates that the protoliths (marine carbonate) of carbonatite went through high temperature process. The

major element contents of garnet and diopside analyzed by are listed in Table S4. The trace element characteristics, as well as oxygen isotope composition, of zircons indicate that these zircons were crystallized in carbonatitic magmas (Fig. 10).

U-Pb dating of zircon rim yields Devonian ages of ~400 Ma, corresponding to the episodes of zircon growth at the end of the Qilian orogeny collision process (440–400 Ma). The zircon cores show an age spectra that has an obvious affiliation with Qilian block but differ from the Longshou Mountain metamorphic basement (Fig. 11). The core age spectra of carbonatite samples show five age peaks (395 Ma, 830 Ma, 1050 Ma, 1600 Ma and 2010 Ma), among which the 400 Ma and 830 Ma peaks are strong evidences that sedimentary materials originated from the Qilian Block. Only the Qilian Block has the detrital zircon peak of 830 Ma, while the Longshou Mountain gneiss and NCC detrital zircons have no such peak. This also suggests that the Taohuala Mountain carbonatite is not a kind of metamorphic marble originated in Longshou Mountain Group.

5.3. Carbon cycle models and geodynamics of Taohuala Mountain carbonatite

Subducted sedimentary carbonates may be recycled back through volcanic activities (Li et al., 2016; Sun and Zhang, 2017; Zhang et al., 2017). During plate subduction, basaltic crust with carbonate vein, overlying calcite-rich sediments and underlying carbon-rich mantle lithospheres may take carbon into the mantle (Alt and Teagle, 1999; Jarrard, 2003). Generally, phase equilibrium experiments and thermodynamic calculation suggests that sedimentary carbonate may remain stable during shallow slab dehydration and possible hydrous melting and could subduct into deep mantle, beyond sub-arc depths (Connolly, 2005; Kerrick and Connolly, 2001a; Kerrick and Connolly, 2001b; Molina and Poli, 2000; Poli et al., 2009; Yaxley and Green, 1994). The solidus temperatures of carbonated basaltic eclogite are crucial to understand the carbon taken by subducted ocean crust. It is influenced by a number of key parameters, such as geothermal gradient of subduction zone and water-bearing contents (Dasgupta et al., 2005; Dasgupta et al., 2004; Hammouda, 2003; Syracuse et al., 2010; van Keken et al., 2002; Yaxley and Brey, 2004). Partial melting of carbonated eclogite assemblages is commonly restricted to hot subduction regimes at high temperatures (> 1050 °C) and high pressures (12–20 GPa, 300–600 km) conditions (Dasgupta and Hirschmann, 2010; Thomson et al., 2016; Wyllie and Tuttle, 1960). Recently, Poli (2015) proposed that the melting temperatures and pressures may be reduced in water-bearing conditions. Calcium-rich hydrous carbonatitic

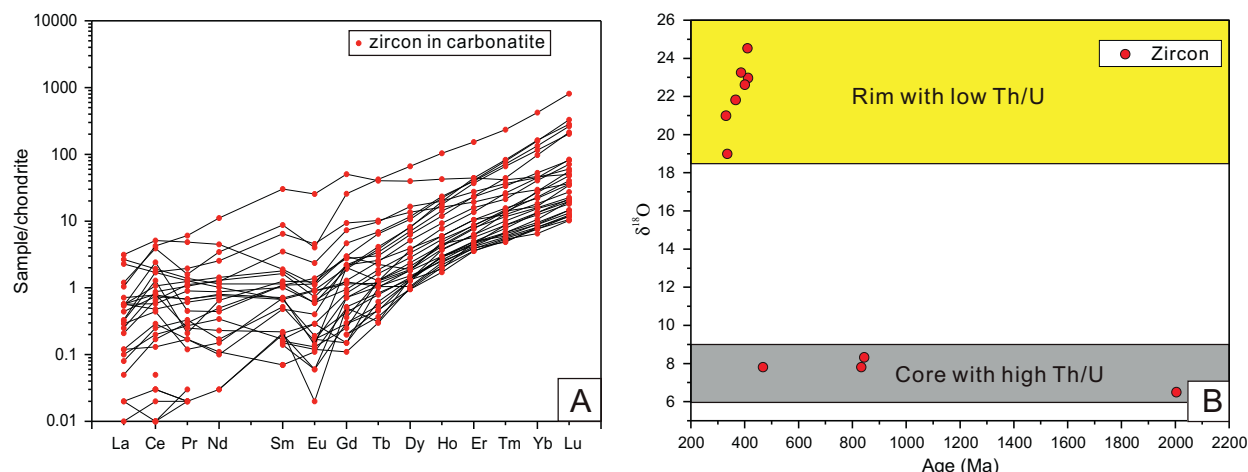


Fig. 10. A: Chondrite-normalized rare earth element (REE) pattern for zircons from carbonatite rocks of the Taohuala Mountain. Chondrite normalization values are from Sun and McDonough (1989). B: The diagram of zircon ages and O isotopic values. Yellow bar indicates the rims (young ages) with high O isotopic values and low Th/U, grey bar represents the cores (old ages) with low O isotopic values and high Th/U. (For interpretation of the references to colour in this figure legend, the reader is referred to the web version of this article.)

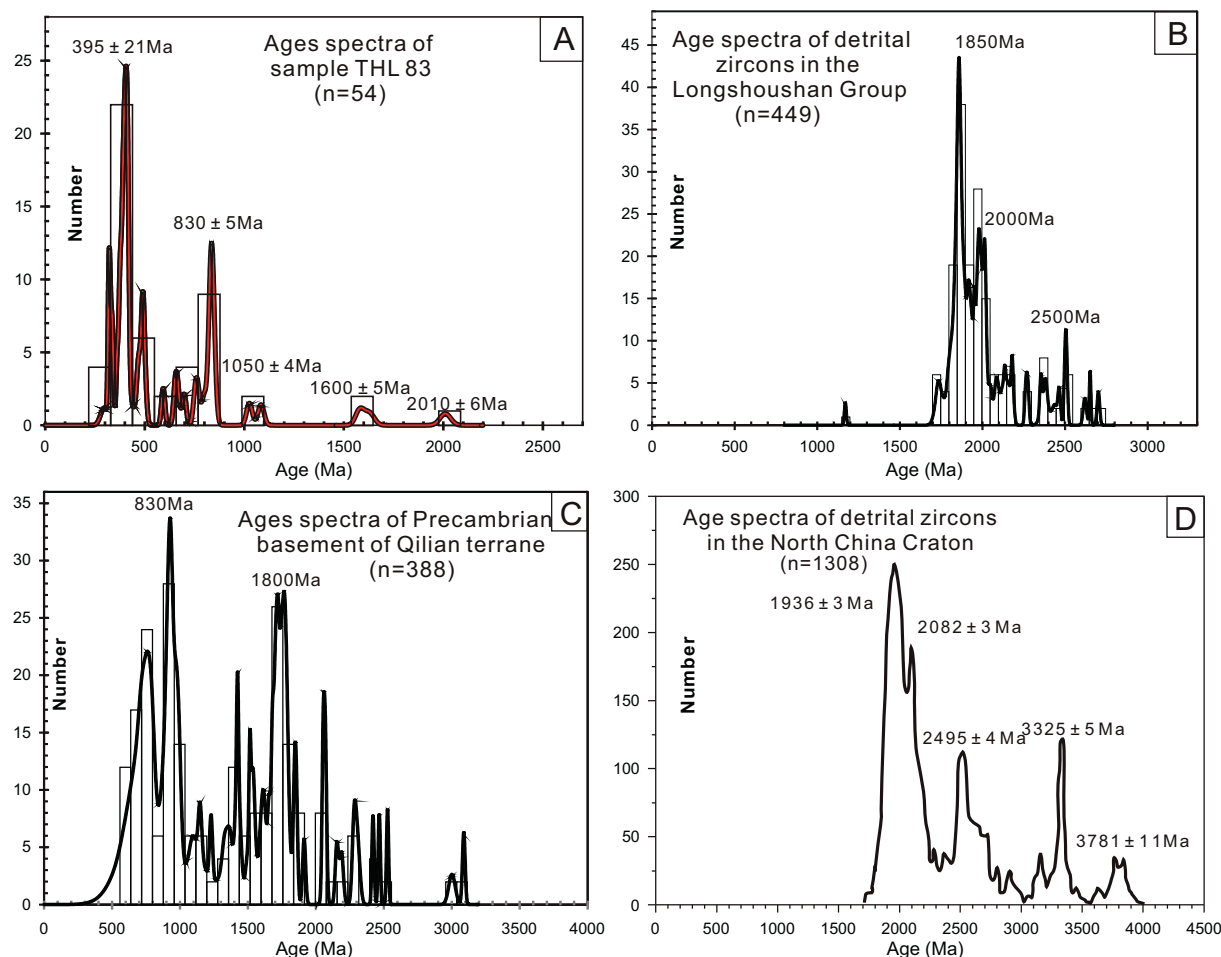


Fig. 11. (A) Age spectra of Taohuala Mountain carbonatite. (B) Compilation of age spectra of Longshou Mountain metamorphic basement. (C) Age spectra of Precambrian basement of Qilian terrane. (D) Compilation of age spectra of the NCC (Modified after Xu et al., 2010 and references therein). Data for (B–C) are from literatures (Gong et al., 2011; Li et al., 2007; Tseng et al., 2006; Tung et al., 2007; Wang et al., 2007; Xu et al., 2007). The degree of concordance is based on the comparison between $^{206}\text{Pb}/^{238}\text{U}$ apparent age and $^{207}\text{Pb}/^{206}\text{Pb}$ apparent age. Ages > 1200 Ma calculated using $^{207}\text{Pb}/^{206}\text{Pb}$ ratios, and ages < 1200 Ma calculated from $^{206}\text{Pb}/^{238}\text{U}$ ratios.

liquids can form at temperatures as low as 870–900 °C, which corresponds to shallower depths of ~120 km beneath subduction zone arcs, in warm subduction regimes. At further depths, carbonated MORB get melted before it goes across the upper-lower mantle boundary (Thomson et al., 2016). Therefore, in general, carbonate cannot be preserved in the mantle as residues of the subducted oceanic slab. Nevertheless, carbonate may be preserved at depths of 300–800 km as carbonated peridotite after react with mantle peridotite (Sun et al., 2017).

The solidus (2–35 GPa) of nominally anhydrous, carbonated peridotite constrained by laboratory partial melting experiments is given by:

$$\begin{aligned} T(\text{°C}) = & 0.0238 \times [P(\text{GPa})]^3 - 2.2084 \times [P(\text{GPa})]^2 + 73.7991 \times P(\text{GPa}) \\ & + 830.3808 \end{aligned}$$

These experiments include those from Falloon and Green (1990) at 1.4–3.5 GPa, Dasgupta and Hirschmann (2006) at 3.0–10.0 GPa, Dasgupta and Hirschmann (2007) at 6.6 GPa, Ghosh et al. (2009) at 10.0–20.0 GPa, and Litasov and Ohtani (2009) at 16.5–32.0 GPa. The carbonated mantle peridotites get melted efficiently at the depth of 50–300 km (2–10 GPa), forming typical carbonatites.

In contrast, the Taohuala Mountain carbonatite is different from such carbon recycling pathway. The Taohuala Mountain carbonatite dykes intruded into the Longshou Mountain gneiss at ~400 Ma, which is roughly at the end of the Qilian orogeny process. According to geological studies, subduction of the North Qilian Ocean started in the

Early Ordovician, with collision along the North Qilian Suture Zone at about 460–440 Ma (Song et al., 2013). Qaidam–Qilian Craton started to subduct beneath the NCC dragged by the downgoing oceanic lithosphere and reached depths > 100 km at 420 Ma. Some early eclogite blocks (oceanic fragments) were entrained by the subducted continental crust. The ultrahigh pressure metamorphosed continental materials started to exhume when the positive buoyancy exceeded the drag of the subducted oceanic lithosphere (i.e. oceanic slab break-off) at ~400 Ma (Song et al., 2009; Song et al., 2006). The formation of the Taohuala Mountain carbonatite is likely related to the post collisional slab rollback and/or slab breakoff (Fig. 12).

From the whole rock C-O-Sr-Nd isotope characteristics, the carbonatite shows a close affiliation with sedimentary carbonates with minor mantle contributions. Considering that the Taohuala Mountain carbonatite was formed right after the collision along the Qilian Mountain, the most likely process is that subducted sedimentary carbonates were piled at shallow depths in the mantle wedge because of lower density and viscosity at the depth of ~100 km similar to previously proposed (Behn et al., 2011; Currie et al., 2007). These carbonates may have been influenced by subduction released fluids, as indicated by its high Ba contents. In the case of the Taohuala Mountain carbonatite, it was formed by partial melting of recycling of subducted sedimentary carbonates rather than carbonated peridotite. The Taohuala Mountain carbonatite has a large proportion of sedimentary carbonate origin, because recycled sedimentary carbonates remained shortly in the mantle and didn't reach isotopic equilibrium with the mantle before

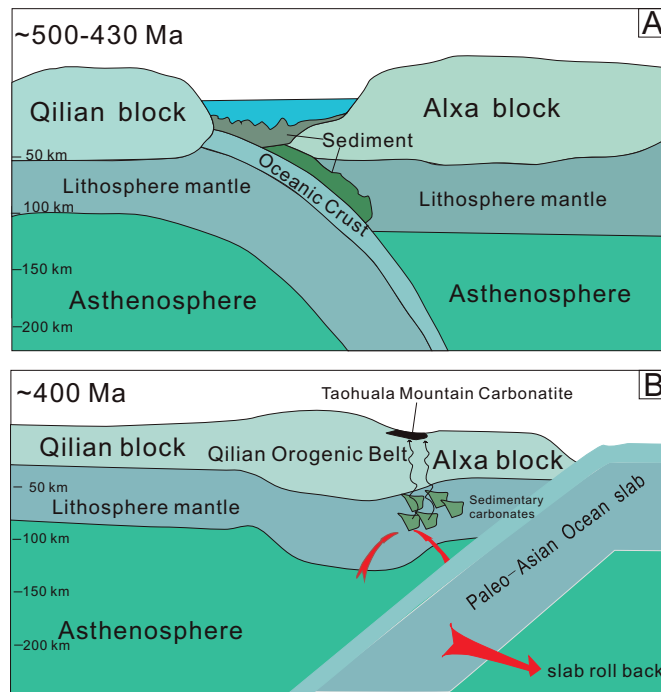


Fig. 12. Geodynamic model of Taohuala Mountain carbonatite.

recycling. The Ca/Mg ratios were not totally reset in this process. Liu et al. (2015) also reported direct evidence of sedimentary carbonate recycling in subduction-related xenoliths from Dalihu (northern China), in which carbonatite melt pockets retain the low trace element concentration and higher $\delta^{18}\text{O}_{\text{VSMOW}} = 21.1 \pm 0.3$ of argillaceous carbonate sediments, similar to the Taohuala Mountain carbonatite. Currie et al. (2007) proposed that a subhorizontal sediment plume develops and intrudes the continental lithosphere owing to their low density during subduction. Partial melting of recycled sedimentary carbonates in the lithospheric mantle may play an important role to generate calciocarbonatitic magmas.

There was a slab rollback after the collision along the Qilian Mountains, as indicated by granitoids (Xue et al., 2017). Subducted carbonates were the first to be partially melted during such slab rollback, because of its low solidus temperature. From this perspective, the Taohuala Mountain carbonatite is a new type of carbonatite, suggesting that some of the subducted carbonates may be recycled at shallow depths (Fig. 12).

6. Conclusion

The Taohuala Mountain carbonatite is characterized by high CaO (45.93–53.86 mass wt%), low SiO₂ (2.37–11.45 wt%) and MgO (0.51–4.39 wt%), enrichment of LILE (Ba, Sr), depletion of HFSE (Nb, Ta, Zr, Hf), and slightly negative Eu anomaly. High $^{87}\text{Sr}/^{86}\text{Sr}$ (0.70686–0.70694) and low $^{143}\text{Nd}/^{144}\text{Nd}$ (0.511635–0.511924), and fractionated $\delta^{18}\text{O}_{\text{VSMOW}}$ (11.83–25.92‰) compositions indicate the involvement of both sedimentary and mantle carbonates. Ages and $\delta^{18}\text{O}_{\text{VSMOW}}$ from core to rim, i.e., old ages (mainly > 800 Ma), high Th/U (mainly > 0.5) and low $\delta^{18}\text{O}_{\text{VSMOW}}$ (6.37–11.44‰) in core, and young ages (~400 Ma), low Th/U (mainly < 0.01) and high $\delta^{18}\text{O}_{\text{VSMOW}}$ (20.04–24.54‰) in rim, suggest that the Taohuala Mountain carbonatite may be generated from partial melting of recycled sedimentary carbonate with minor mantle contribution at shallow depths.

We propose that sedimentary carbonates subducted and retained beneath the Alxa continental lithosphere at depths of ~100 km during the closure of the Paleo-Qilian Ocean. Subsequently, the Taohuala

Mountain carbonatite was formed by melting of the carbonates during the breakoff or rollback of the Paleo-Asian oceanic slab.

Supplementary data to this article can be found online at <https://doi.org/10.1016/j.chemgeo.2017.10.039>.

Acknowledgements

We would like to thank Prof. Klaus Mezger and two anonymous reviewers for the handling and constructive review comments on our manuscript. This work was supported by National Key R & D Program of China (2017YFC0602301 and 2017YFC0602302), Guangdong Natural Science Funds (2014A030306032 and 2015TQ01Z611), Natural Science Foundation of China (41421062) and Youth Innovation Promotion Association CAS (2016315). This is contribution No. IS-2462 from GIGCAS.

References

- Alt, J.C., Teagle, D.A.H., 1999. The uptake of carbon during alteration of ocean crust. *Geochim. Cosmochim. Acta* 63, 1527–1535.
- Bai, G., Yuan, Z., 1985. Carbonatites and related mineral resources. *Bull. Inst. Mineral Deposits Chin. Acad. Geol. Sci.* 13, 1–193 (in Chinese with English abstract).
- Barker, D.S., 1996. Consequences of recycled carbon in carbonatites. *Can. Mineral.* 34, 373–387.
- Behn, M.D., Kelemen, P.B., Hirth, G., Hacker, B.R., Massonne, H.J., 2011. Diaps as the source of the sediment signature in arc lavas. *Nat. Geosci.* 4, 641–646.
- Bell, K., Simonetti, A., 2010. Source of parental melts to carbonatites—critical isotopic constraints. *Mineral. Petrol.* 98, 77–89.
- Bellanca, A., Masetti, D., Neri, R., 1997. Rare earth elements in limestone/marlstone couples from the Albion-Cenomanian Cismon section (Venetian region, northern Italy): assessing REE sensitivity to environmental changes. *Chem. Geol.* 141, 141–152.
- Chakhrouradian, A.R., 2006. High-field-strength elements in carbonatitic rocks: geochemistry, crystal chemistry and significance for constraining the sources of carbonatites. *Chem. Geol.* 235, 138–160.
- Chen, W., Simonetti, A., 2013. In-situ determination of major and trace elements in calcite and apatite, and U-Pb ages of apatite from the Oka carbonatite complex: insights into a complex crystallization history. *Chem. Geol.* 353, 151–172.
- Chen, Z.H., Li, C., Qu, W.J., Wang, D.H., Zhang, J.J., Du, A.D., 2010. Research and preliminary application in metallogenic chronology of Re-Os isotope system in graphite samples. *Acta Petrol. Sin.* 26, 3411–3417 (in Chinese with English abstract).
- Chen, C., Liu, Y., Foley, S.F., Ducea, M.N., He, D., Hu, Z., Chen, W., Zong, K., 2016. Paleo-Asian oceanic slab under the North China craton revealed by carbonatites derived from subducted limestones. *Geology* 44, 1039–1042.
- Chew, D.M., Sylvester, P.J., Tubrett, M.N., 2011. U-Pb and Th-Pb dating of apatite by LA-ICPMS. *Chem. Geol.* 280, 200–216.
- Connolly, J.A.D., 2005. Computation of phase equilibria by linear programming: a tool for geodynamic modeling and its application to subduction zone decarbonation. *Earth Planet. Sci. Lett.* 236, 524–541.
- Cui, Q., 1976. Geological characteristics and genesis of a Nb deposit in Gansu. *Northwest Geol.* 30–36 (in Chinese with English abstract).
- Currie, C.A., Beaumont, C., Huismans, R.S., 2007. The fate of subducted sediments: a case for backarc intrusion and underplating. *Geology* 35, 1111–1114.
- Dan, W., Li, X.H., Wang, Q., Tang, G.J., Liu, Y., 2014. An Early Permian (ca. 280 Ma) silicic igneous province in the Alxa Block, NW China: a magmatic flare-up triggered by a mantle-plume? *Lithos* 204, 144–158.
- Dasgupta, R., Hirschmann, M.M., 2006. Melting in the Earth's deep upper mantle caused by carbon dioxide. *Nature* 440, 659–662.
- Dasgupta, R., Hirschmann, M.M., 2007. Effect of variable carbonate concentration on the solidus of mantle peridotite. *Am. Mineral.* 92, 370–379.
- Dasgupta, R., Hirschmann, M.M., 2010. The deep carbon cycle and melting in Earth's interior. *Earth Planet. Sci. Lett.* 298, 1–13.
- Dasgupta, R., Hirschmann, M.M., Withers, A.C., 2004. Deep global cycling of carbon constrained by the solidus of anhydrous, carbonated eclogite under upper mantle conditions. *Earth Planet. Sci. Lett.* 227, 73–85.
- Dasgupta, R., Hirschmann, M.M., Dellas, N., 2005. The effect of bulk composition on the solidus of carbonated eclogite from partial melting experiments at 3 GPa. *Contrib. Mineral. Petrol.* 149, 288–305.
- Dawson, J.B., Steele, I.M., Smith, J.V., Rivers, M.L., 1996. Minor and trace element chemistry of carbonates, apatites and magnetites in some African carbonatites. *Mineral. Mag.* 60, 415–425.
- Demény, A., Ahijado, A., Casillas, R., Vennemann, T.W., 1998. Crustal contamination and fluid/rock interaction in the carbonatites of Fuerteventura (Canary Islands, Spain): a C, O, H isotope study. *Lithos* 44, 101–115.
- Falloon, T.J., Green, D.H., 1990. Solidus of carbonated fertile peridotite under fluid-saturated conditions. *Geology* 18, 195–199.
- Fan, H.R., Yang, K.F., Hu, F.F., Liu, S., Wang, K.Y., 2016. The giant Bayan Obo REE-Nb-Fe deposit, China: controversy and ore genesis. *Geosci. Front.* 7, 335–344.
- Feng, J., Xiao, W., Windley, B., Han, C., Wan, B., Zhang, J.e., Ao, S., Zhang, Z., Lin, L., 2013. Field geology, geochronology and geochemistry of mafic-ultramafic rocks from

- Alxa, China: implications for Late Permian accretionary tectonics in the southern Altaiids. *J. Asian Earth Sci.* 78, 114–142.
- Geng, Y., Zhou, X., 2012. Early Permian magmatic events in the Alxa metamorphic basement: evidence from geochronology. *Acta Petrol. Sin.* 28, 2667–2685 (in Chinese with English abstract).
- Ghosh, S., Ohtani, E., Litasov, K.D., Terasaki, H., 2009. Solidus of carbonated peridotite from 10 to 20 GPa and origin of magnesiocarbonate melt in the Earth's deep mantle. *Chem. Geol.* 262, 17–28.
- Gong, J., Zhang, J., Yu, S., 2011. The origin of Longshoushan Group and associated rocks in the southern part of the Alxa block: constraint from LA-ICP-MS U-Pb zircon dating. *Acta Petrol. Mineral.* 30, 795–818 (in Chinese with English abstract).
- Guan, Q., Zhu, D.C., Zhao, Z.D., Zhang, L.L., Liu, M., Li, X.W., Yu, F., Mo, X.X., 2010. Late Cretaceous adakites in the eastern segment of the Gangdese Belt, southern Tibet: products of Neo-Tethyan ridge subduction? *Acta Petrol. Sin.* 26, 2165–2179 (in Chinese with English abstract).
- Halama, R., Vennemann, T., Siebel, W., Markl, G., 2005. The Gronnedal-Ika carbonatite-syenite complex, South Greenland: carbonatite formation by liquid immiscibility. *J. Petrol.* 46, 191–217.
- Halama, R., McDonough, W.F., Rudnick, R.L., Bell, K., 2008. Tracking the lithium isotopic evolution of the mantle using carbonatites. *Earth Planet. Sci. Lett.* 265, 726–742.
- Hammouda, T., 2003. High-pressure melting of carbonated eclogite and experimental constraints on carbon recycling and storage in the mantle. *Earth Planet. Sci. Lett.* 214, 357–368.
- Harmer, R.E., Gittins, J., 1998. The case for primary, mantle-derived carbonatite magma. *J. Petrol.* 39, 1895–1903.
- Hoernle, K., Tilton, G., Le Bas, M.J., Duggen, S., Garbe-Schonberg, D., 2002. Geochemistry of oceanic carbonatites compared with continental carbonatites: mantle recycling of oceanic crustal carbonate. *Contrib. Mineral. Petrol.* 142, 520–542.
- Hou, Z.Q., Tian, S.H., Yuan, Z.X., Xie, Y.L., Yin, S.P., Yi, L.S., Fei, H.C., Yang, Z.M., 2006. The Himalayan collision zone carbonatites in western Sichuan, SW China: petrogenesis, mantle source and tectonic implication. *Earth Planet. Sci. Lett.* 244, 234–250.
- Hou, Z.Q., Liu, Y., Tian, S.H., Yang, Z.M., Xie, Y.L., 2015. Formation of carbonatite-related giant rare-earth-element deposits by the recycling of marine sediments. *Sci. Rep.* 5. <http://dx.doi.org/10.1038/srep10231>.
- Ivanov, K.S., Valizor, P.M., Erokhin, Y.V., Pogromskaya, O.E., 2010. Genesis of carbonatites of fold belts (exemplified by the Urals). *Dokl. Earth Sci.* 435, 1423–1426.
- Jarrard, R.D., 2003. Subduction fluxes of water, carbon dioxide, chlorine, and potassium. *Geochem. Geophys. Geosyst.* 4. <http://dx.doi.org/10.1029/2002GC000392>.
- Jiang, R.L., 1989. Inner Mongolia Ayu Banner Taohuala Mountain rear, rear earth ore deposit geological characteristics and occurrence regularity. *Northwest. Geol.* 41–48 (in Chinese with English abstract).
- Jin, Z.J., Zhu, D.Y., Hu, W.X., Zhang, X.F., Zhang, J.T., Song, Y.C., 2009. Mesogenetic dissolution of the middle Ordovician limestone in the Tahe oilfield of Tarim basin, NW China. *Mar. Pet. Geol.* 26, 753–763 (in Chinese with English abstract).
- Jones, J.H., Walker, D., Pickett, D.A., Murrell, M.T., Beattie, P., 1995. Experimental investigations of the partitioning of Nb, Mo, Ba, Ce, Pb, Ra, Th, Pa, and U between immiscible carbonate and silicate liquids. *Geochim. Cosmochim. Acta* 59, 1307–1320.
- van Keken, P.E., Kiefer, B., Peacock, S.M., 2002. High-resolution models of subduction zones: implications for mineral dehydration reactions and the transport of water into the deep mantle. *Geochem. Geophys. Geosyst.* 3. <http://dx.doi.org/10.1029/2001GC000256>.
- Keller, J., Hoefs, J., 1995. Stable Isotope Characteristics of Recent Natrocarbonatites from Oldoinyo Lengai. In: Bell, K., Keller, J. (Eds.), *Carbonatite Volcanism: Oldoinyo Lengai and the Petrogenesis of Natrocarbonatites*. Springer Berlin Heidelberg, Berlin, Heidelberg, pp. 113–123.
- Kerrick, D.M., Connolly, J.A.D., 2001a. Metamorphic devolatilization of subducted marine sediments and the transport of volatiles into the Earth's mantle. *Nature* 411, 293–296.
- Kerrick, D.M., Connolly, J.A.D., 2001b. Metamorphic devolatilization of subducted oceanic metabasalts: implications for seismicity, arc magmatism and volatile recycling. *Earth Planet. Sci. Lett.* 189, 19–29.
- Lai, X., Jiang, S., Qiu, X., Liu, Y., Hu, P., Zhang, W., 2007. ^{40}Ar - ^{39}Ar Age and geochemical features of Hercynian intermediate acidic rock in Beidashan Rock Belt, Alxa. *Acta Geol. Sin.* 81, 370–380 (in Chinese with English abstract).
- Li, J.J., 2006. Regional Metallogenetic System of Alashan Block in Inner Mongolia Autonomous Region. China University of Geosciences, Beijing (in Chinese with English abstract).
- Li, H., Lu, S., Xiang, Z., Zhou, H., Li, H., Liu, D., Song, B., Zheng, J., Gu, Y., 2007. SHRIMP U-Pb geochronological research on detrital zircons from the Beidahei complex-group in the western segment of the North Qilian Mountains, Northwest China. *Geol. Rev.* 53, 132–140 (in Chinese with English abstract).
- Li, X.H., Liu, Y., Li, Q.L., Guo, C.H., Chamberlain, K.R., 2009. Precise determination of Phanerozoic zircon Pb/Pb age by multicollector SIMS without external standardization. *Geochem. Geophys. Geosyst.* 10. <http://dx.doi.org/10.1029/2009GC002400>.
- Li, J., Zhai, Y., Sang, H., Li, H., Zhang, Y., Liu, S., Wang, S., Sun, Z., Liu, X., 2010a. Metallogenetic epoch of the Oubulage copper-gold deposit in the Alashan area, Inner Mongolia Autonomous Region. *Bull. Mineral. Petrol. Geochem.* 29, 323–327 (in Chinese with English abstract).
- Li, X.H., Long, W.G., Li, Q.L., Liu, Y., Zheng, Y.F., Yang, Y.H., Chamberlain, K.R., Wan, D.F., Guo, C.H., Wang, X.C., Tao, H., 2010b. Penglai zircon megacrysts: a potential new working reference material for microbeam determination of Hf-O isotopes and U-Pb age. *Geostand. Geoanal. Res.* 34, 117–134.
- Li, S.-G., Yang, W., Ke, S., Meng, X., Tian, H., Xu, L., He, Y., Huang, J., Wang, X.-C., Xia, Q., 2016. Deep carbon cycles constrained by a large-scale mantle Mg isotope anomaly in eastern China. *Nat. Sci. Rev.* 4, 111–120.
- Liang, X., Wei, G., Li, X., Liu, Y., 2003. Precise measurement of $^{143}\text{Nd}/^{144}\text{Nd}$ and Sm/Nd ratios using multiple-collectors inductively coupled plasma-mass spectrometer (MC-ICPMS). *Geochimica* 32, 91–96 (in Chinese with English abstract).
- Ling, M.X., Liu, Y.L., Williams, I.S., Teng, F.Z., Yang, X.Y., Ding, X., Wei, G.J., Xie, L.H., Deng, W.F., Sun, W.D., 2013. Formation of the world's largest REE deposit through protracted fluxing of carbonatite by subduction-derived fluids. *Sci. Rep.* 3. <http://dx.doi.org/10.1038/srep01776>.
- Litasov, K.D., Ohtani, E., 2009. Solidus and phase relations of carbonated peridotite in the system CaO-Al₂O₃-MgO-SiO₂-Na₂O-CO₂ to the lower mantle depths. *Phys. Earth Planet. Inter.* 177, 46–58.
- Liu, H.Y., Montaser, A., Dolan, S.P., Schwartz, R.S., 1996. Evaluation of a low sample consumption, high-efficiency nebulizer for elemental analysis of biological samples using inductively coupled plasma mass spectrometry. *J. Anal. At. Spectrom.* 11, 307–311.
- Liu, Y.L., Williams, I.S., Chen, J.F., Wan, Y.S., Sun, W.D., 2008. The significance of paleoproterozoic zircon in carbonatite dikes associated with the bayan obo REE-Nb-Fe deposit. *Am. J. Sci.* 308, 379–397.
- Liu, Y.C., Liu, L.X., Gu, X.F., Li, S.G., Liu, J., Song, B.A., 2010. Occurrence of Neoproterozoic low-grade metagranite in the western Beihuiyang zone, the Dabie orogen. *Chin. Sci. Bull.* 55, 3490–3498.
- Liu, Y.S., He, D.T., Gao, C.G., Foley, S., Gao, S., Hu, Z.C., Zong, K.Q., Chen, H.H., 2015. First direct evidence of sedimentary carbonate recycling in subduction-related xenoliths. *Sci. Rep.* 5. <http://dx.doi.org/10.1038/srep11547>.
- Lu, Z., Bucher, K., Zhang, L.F., 2013. Omphacite-bearing calcite marble and associated coesite-bearing pelitic schist from the meta-ophiolitic belt of Chinese western Tianshan. *J. Asian Earth Sci.* 76, 37–47.
- Ludwig, K., 2012. User's manual for Isoplot version 3.75–4.15: a geochronological toolkit for Microsoft. In: Excel Berkley Geochronological Center Special Publication.
- Ma, J.L., Wei, G.J., Xu, Y.G., Long, W.G., Sun, W.D., 2007. Mobilization and re-distribution of major and trace elements during extreme weathering of basalt in Hainan Island, South China. *Geochim. Cosmochim. Acta* 71, 3223–3237.
- Martin, L.H.J., Schmidt, M.W., Mattsson, H.B., Guenther, D., 2013. Element partitioning between immiscible carbonatite and silicate melts for dry and H₂O-bearing systems at 1–3 GPa. *J. Petrol.* 54, 2301–2338.
- Mitchell, R.H., 2005. Carbonatites and carbonatites and carbonatites. *Can. Mineral.* 43, 2049–2068.
- Molina, J.F., Poli, S., 2000. Carbonate stability and fluid composition in subducted oceanic crust: an experimental study on H₂O-CO₂-bearing basalts. *Earth Planet. Sci. Lett.* 176, 295–310.
- Moser, D.E., Bowman, J.R., Wooden, J., Valley, J.W., Mazdab, F., Kita, N., 2008. Creation of a continent recorded in zircon zoning. *Geology* 36, 239–242.
- Page, F.Z., Ushikubo, T., Kita, N.T., Ricupi, L.R., Valley, J.W., 2007. High-precision oxygen isotope analysis of picogram samples reveals 2 mu m gradients and slow diffusion in zircon. *Am. Mineral.* 92, 1772–1775.
- Peck, W.H., Valley, J.W., Graham, C.M., 2003. Slow oxygen diffusion rates in igneous zircons from metamorphic rocks. *Am. Mineral.* 88, 1003–1014.
- Poli, S., 2015. Carbon mobilized at shallow depths in subduction zones by carbonatitic liquids. *Nat. Geosci.* 8, 633–636.
- Poli, S., Franzolin, E., Fumagalli, P., Crottini, A., 2009. The transport of carbon and hydrogen in subducted oceanic crust: an experimental study to 5 GPa. *Earth Planet. Sci. Lett.* 278, 350–360.
- Qin, J.F., Lai, S.C., Diwu, C.R., Ju, Y.J., Li, Y.F., 2010a. Magma mixing origin for the post-collisional adakitic monzogranite of the Triassic Yangba pluton, northwestern margin of the South China block: geochemistry, Sr-Nd isotopic, zircon U-Pb dating and Hf isotopic evidences. *Contrib. Mineral. Petrol.* 159, 389–409.
- Qin, J.F., Lai, S.C., Grapes, R., Diwu, C.R., Ju, Y.J., Li, Y.F., 2010b. Origin of Late Triassic high-Mg adakitic granitoid rocks from the Dongjiangkou area, Qinling orogen, central China: implications for subduction of continental crust. *Lithos* 120, 347–367.
- Ran, H., Zhang, W., Liu, Z., 2012. Geochemical characteristics and LA-ICP-MS zircon U-Pb dating of the Late Permian monzogranite in Hanggale, Alxa Right Banner, Inner Mongolia. *Geol. Bull. China* 31, 1565–1575 (in Chinese with English abstract).
- Rukhlov, A.S., Bell, K., 2010. Geochronology of carbonatites from the Canadian and Baltic shields, and the Canadian cordilleran: clues to mantle evolution. *Mineral. Petrol.* 98, 11–54.
- Shi, X., Tong, Y., Wang, T., Zhang, J., Zhang, Z., Zhang, L., Guo, L., Zeng, T., Geng, J., 2012. LA-ICP-MS zircon U-Pb age and geochemistry of the Early Permian Halinludeng granite in northern Alxa area, western Inner Mongolia. *Geol. Bull. China* 31, 662–670 (in Chinese with English abstract).
- Song, S.G., Zhang, L.F., Niu, Y.L., Su, L., Song, B.A., Liu, D.Y., 2006. Evolution from oceanic subduction to continental collision: a case study from the northern Tibetan Plateau based on geochemical and geochronological data. *J. Petrol.* 47, 435–455.
- Song, S.G., Niu, Y.L., Zhang, L.F., Wei, C.J., Liou, J.G., Su, L., 2009. Tectonic evolution of early Paleozoic HP metamorphic rocks in the North Qilian Mountains, NW China: new perspectives. *J. Asian Earth Sci.* 35, 334–353.
- Song, S.G., Niu, Y.L., Su, L., Xia, X.H., 2013. Tectonics of the North Qilian orogen, NW China. *Gondwana Res.* 23, 1378–1401.
- Song, W.L., Xu, C., Smith, M.P., Kynicky, J., Huang, K.J., Wei, C.W., Zhou, L., Shu, Q.H., 2016. Origin of unusual HREE-Mo-rich carbonatites in the Qinling orogen, China. *Sci. Rep.* 6. <http://dx.doi.org/10.1038/srep37377>.
- Stacey, J.S., Kramers, J.D., 1975. Approximation of terrestrial lead isotope evolution by a 2-stage model. *Earth Planet. Sci. Lett.* 26, 207–221.
- Sun, S.-S., McDonough, W., 1989. Chemical and isotopic systematics of oceanic basalts: implications for mantle composition and processes. *Geol. Soc. Lond. Spec. Publ.* 42, 313–345.

- Sun, W.-D., Zhang, C.-C., 2017. Carbon recycling through alkali basalts. *Solid Earth Sci.* 2, 41–42. <http://dx.doi.org/10.1016/j.sesci.2017.03.002>.
- Sun, J.F., Yang, J.H., Wu, F.Y., Li, X.H., Yang, Y.H., Xie, L.W., Wilde, S.A., 2010. Magma mixing controlling the origin of the Early Cretaceous Fangshan granitic pluton, North China craton *in situ* U-Pb age and Sr-, Nd-, Hf- and O-isotope evidence. *Lithos* 120, 421–438.
- Sun, W.-D., Hawkesworth, C.J., Yao, C., Zhang, C.-C., Huang, R.-F., Liu, X., Sun, X.-L., Ireland, T., Song, M.-S., Ling, M.-X., Ding, X., Zhang, Z.-F., Fan, W.-M., Wu, Z.-Q., 2017. Carbonated mantle domains at the base of the Earth's transition zone. *Chem. Geol.* <http://dx.doi.org/10.1016/j.chemgeo.2017.08.001>.
- Sweeney, R.J., 1994. Carbonate melt compositions in the earth's mantle. *Earth Planet. Sci. Lett.* 128, 259–270.
- Syracuse, E.M., van Keeken, P.E., Abers, G.A., 2010. The global range of subduction zone thermal models. *Phys. Earth Planet. Inter.* 183, 73–90.
- Tanaka, K., Miura, N., Asahara, Y., Kawabe, I., 2003. Rare earth element and strontium isotopic study of seamount-type limestones in Mesozoic accretionary complex of Southern Chichibit terrane, central Japan: implication for incorporation process of seawater REE into limestones. *Geochem. J.* 37, 163–180.
- Tappe, S., Steenfelt, A., Nielsen, T., 2012. Asthenospheric source of Neoproterozoic and Mesozoic kimberlites from the North Atlantic craton, West Greenland: new high-precision U-Pb and Sr-Nd isotope data on perovskite. *Chem. Geol.* 320, 113–127.
- Taylor, H.P., Frechen, J., Degens, E.T., 1967. Oxygen and carbon isotope studies of carbonates from the Laacher See District, West Germany and the Alnö District, Sweden. *Geochim. Cosmochim. Acta* 31, 407–430.
- Thomson, A.R., Walter, M.J., Kohn, S.C., Brooker, R.A., 2016. Slab melting as a barrier to deep carbon subduction. *Nature* 529, 76–79.
- Tseng, C.-Y., Yang, H.-Y., Yusheng, W., Dunyi, L., Wen, D.-J., Lin, T.-C., Tung, K.-A., 2006. Finding of Neoproterozoic (~775 Ma) magmatism recorded in metamorphic complexes from the North Qilian orogen: evidence from SHRIMP zircon U-Pb dating. *Chin. Sci. Bull.* 51, 963–970.
- Tsikos, H., Moore, J.M., Harris, C., 2001. Geochemistry of the Palaeoproterozoic Moodraai formation: Fe-rich limestone as end member of iron formation deposition, Kalahari manganese field, Transvaal Supergroup, South Africa. *J. Afr. Earth Sci.* 32, 19–27.
- Tung, K., Yang, H., Liu, D., Zhang, J., Tseng, C., Wan, Y., 2007. SHRIMP U-Pb geochronology of the detrital zircons from the Longshoushan Group and its tectonic significance. *Chin. Sci. Bull.* 52, 1414–1425.
- Valley, J.W., 2003. Oxygen isotopes in zircon. *Rev. Mineral. Geochem.* 53, 343–385.
- Valley, J.W., Chiarenzelli, J.R., McLellan, J.M., 1994. Oxygen-isotope geochemistry of zircon. *Earth Planet. Sci. Lett.* 126, 187–206.
- Van Groo, A.K., Wyllie, P., 1963. Experimental data bearing on the role of liquid immiscibility in the genesis of carbonates. *Nature* 199, 801–802.
- Veizer, J., Ala, D., Azmy, K., Bruckschen, P., Buhl, D., Bruhn, F., Carden, G.A.F., Diener, A., Ebnet, S., Godderis, Y., Jasper, T., Korte, C., Pawellek, F., Podlaha, O.G., Strauss, H., 1999. $^{87}\text{Sr}/^{86}\text{Sr}$, ^{81}O and ^{18}O evolution of Phanerozoic seawater. *Chem. Geol.* 161, 59–88.
- Veksler, I.V., Nielsen, T.F.D., Sokolov, S.V., 1998. Mineralogy of crystallized melt inclusions from Gardiner and Kovdor ultramafic alkaline complexes: implications for carbonate genesis. *J. Petrol.* 39, 2015–2031.
- Veksler, I.V., Dorfman, A.M., Dulski, P., Kamenetsky, V.S., Danyushevsky, L.V., Jeffries, T., Dingwell, D.B., 2012. Partitioning of elements between silicate melt and immiscible fluoride, chloride, carbonate, phosphate and sulfate melts, with implications to the origin of natrocarbonatite. *Geochim. Cosmochim. Acta* 79, 20–40.
- Verhulst, A., Balaganskaya, E., Kirnarovsky, Y., Demaiffe, D., 2000. Petrological and geochemical (trace elements and Sr-Nd isotopes) characteristics of the Paleozoic Kovdor ultramafic, alkaline and carbonatite intrusion (Kola Peninsula, NW Russia). *Lithos* 51, 1–25.
- Wang, H., He, S., Chen, J., Xu, X., Song, Y., Diwu, C., 2007. LA-ICPMS dating of zircon U-Pb and its tectonic significance of Maxianshan granitoid intrusive complex, Gansu Province. *Acta Geographica Sinica - Eng. Ed.* 81, 72.
- Wang, Q., Wyman, D.A., Li, Z.X., Sun, W.D., Chung, S.L., Vasconcelos, P.M., Zhang, Q.Y., Dong, H., Yu, Y.S., Pearson, N., Qiu, H.N., Zhu, T.X., Feng, X.T., 2010. Eocene north-south trending dikes in central Tibet: new constraints on the timing of east-west extension with implications for early plateau uplift? *Earth Planet. Sci. Lett.* 298, 205–216.
- Watson, E.B., Cherniak, D.J., 1997. Oxygen diffusion in zircon. *Earth Planet. Sci. Lett.* 148, 527–544.
- Wei, G., Liang, X., Li, X., Liu, Y., 2002. Precise measurement of Sr isotopic composition of liquid and solid base using (LP) MC-ICPMS. *Geochimica* 31, 295–305 (in Chinese with English abstract).
- Wiedenbeck, M., Rhede, D., Lieckefett, R., Witzki, H., 2004. Cryogenic SIMS and its applications in the earth sciences. *Appl. Surf. Sci.* 231, 888–892.
- Woodard, J., Huhma, H., 2015. Paleoproterozoic mantle enrichment beneath the Fennoscandian shield: isotopic insight from carbonates and lamprophyres. *Lithos* 236, 311–323.
- Woodhead, J.D., 1996. Extreme HIMU in an oceanic setting: the geochemistry of Mangaia Island (Polynesia), and temporal evolution of the cook-austral hotspot. *J. Volcanol. Geotherm. Res.* 72, 1–19.
- Woolley, A., 1989. The Spatial and Temporal Distribution of Carbonatites. *Carbonatites: Genesis and Evolution*. Unwin Hyman, London, pp. 15–37.
- Woolley, A.R., Kjarsgaard, B.A., 2008. Carbonatite occurrences of the world: map and database. *Geol. Surv. Can (Open File 5796)*.
- Wu, K., 2011. *Geochemical Characteristics and Tectonic Setting of Late Varisian Period in Alashan Block*. Chang'an University Xi'an (Master thesis, 70p in Chinese with English abstract).
- Wyllie, P.J., Tuttle, O.F., 1960. The system $\text{CaO}-\text{CO}_2-\text{H}_2\text{O}$ and the origin of carbonatites. *J. Petrol.* 1, 1–46.
- Xia, X., Song, S., Niu, Y., 2012. Tholeiite–Boninite terrane in the North Qilian suture zone: implications for subduction initiation and back-arc basin development. *Chem. Geol.* 328, 259–277.
- Xu, W., Zhang, H., Liu, X., 2007. U-Pb zircon dating constraints on formation time of Qilian high-grade metamorphic rock and its tectonic implications. *Chin. Sci. Bull.* 52, 531–538.
- Xu, Y., Du, Y., Cawood, P.A., Yang, J., 2010. Provenance record of a foreland basin: detrital zircon U-Pb ages from Devonian strata in the North Qilian Orogenic Belt, China. *Tectonophysics* 495, 337–347.
- Xu, C., Kynicky, J., Chakhmouradian, A.R., Li, X.H., Song, W.L., 2015. A case example of the importance of multi-analytical approach in deciphering carbonatite petrogenesis in South Qinling orogen: Miaoya rare-metal deposit, central China. *Lithos* 227, 107–121.
- Xue, S., Ling, M.-X., Liu, Y.-L., Zhang, H., Sun, W., 2017. The genesis of early Carboniferous adakitic rocks at the southern margin of the Alxa Block, North China. *Lithos* 278, 181–194.
- Yang, X.M., Le Bas, M.J., 2004. Chemical compositions of carbonate minerals from Bayan Obo, Inner Mongolia, China: implications for petrogenesis. *Lithos* 72, 97–116.
- Yang, Z.M., Woolley, A., 2006. Carbonatites in China: a review. *J. Asian Earth Sci.* 27, 559–575.
- Yang, X.Y., Sun, W.D., Zhang, Y.X., Zheng, Y.F., 2009. Geochemical constraints on the genesis of the Bayan Obo Fe-Nb-REE deposit in Inner Mongolia, China. *Geochim. Cosmochim. Acta* 73, 1417–1435.
- Yang, W., Teng, F.Z., Zhang, H.F., Li, S.G., 2012. Magnesium isotopic systematics of continental basalts from the North China craton: implications for tracing subducted carbonate in the mantle. *Chem. Geol.* 328, 185–194.
- Yang, X.Y., Lai, X.Y., Pirajno, F., Liu, Y.L., Ling, M.X., Sun, W.D., 2017. Genesis of the Bayan Obo Fe-REE-Nb formation in Inner Mongolia, North China craton: a perspective review. *Precambrian Res.* 288, 39–71.
- Yaxley, G.M., Brey, G.P., 2004. Phase relations of carbonate-bearing eclogite assemblages from 2.5 to 5.5 GPa: implications for petrogenesis of carbonatites. *Contrib. Mineral. Petrol.* 146, 606–619.
- Yaxley, G.M., Green, D.H., 1994. Experimental demonstration of refractory carbonate-bearing eclogite and siliceous melt in the subduction regime. *Earth Planet. Sci. Lett.* 128, 313–325.
- Zhang, Z.C., 1990. Prospecting potential of Longshou mountain in Nb-Ta-REE deposits profiles. *Northwest. Geol.* 4, 13–17 (in Chinese with English abstract).
- Zhang, J.X., Mattinson, C.G., Yu, S.Y., Li, J.P., Meng, F.C., 2010. U-Pb zircon geochronology of coesite-bearing eclogites from the southern Dulan area of the North Qaidam UHP terrane, northwestern China: spatially and temporally extensive UHP metamorphism during continental subduction. *J. Metamorph. Geol.* 28, 955–978.
- Zhang, W., Wu, T.R., Feng, J.C., Zheng, R.G., He, Y.K., 2013. Time constraints for the closing of the paleo-Asian Ocean in the northern Alxa region: evidence from Wuliji granites. *Sci. China - Earth Sci.* 56, 153–164.
- Zhang, G.-L., Chen, L.-H., Jackson, M.G., Hofmann, A.W., 2017. Evolution of carbonated melt to alkali basalt in the South China Sea. *Nat. Geosci.* 10, 229–235.
- Zheng, R.G., Wu, T.R., Zhang, W., Xu, C., Meng, Q.P., 2013. Late Paleozoic subduction system in the southern Central Asian Orogenic Belt: evidences from geochronology and geochemistry of the Xiaohuangshan ophiolite in the Beishan orogenic belt. *J. Asian Earth Sci.* 62, 463–475.
- Zheng, R.G., Wu, T.R., Zhang, W., Xu, C., Meng, Q.P., Zhang, Z.Y., 2014. Late Paleozoic subduction system in the northern margin of the Alxa block, Altaiids: geochronological and geochemical evidences from ophiolites. *Gondwana Res.* 25, 842–858.
- Zhou, X.C., Zhang, H.F., Luo, B.J., Pan, F.B., Zhang, S.S., Guo, L., 2016. Origin of high Sr/Y-type granitic magmatism in the southwestern of the Alxa Block, Northwest China. *Lithos* 256, 211–227.